Title

Disruption of the intestinal clock drives dysbiosis and impaired barrier function in colorectal cancer

Journal

Science Advances, 10(39)

ISSN

2375-2548

Authors

Fellows, Rachel C

Chun, Sung Kook

Larson, Natalie

et al.

Publication Date

2024-09-27

DOI

10.1126/sciadv.ado1458

Peer reviewed

CANCER

Disruption of the intestinal clock drives dysbiosis and impaired barrier function in colorectal cancer

Rachel C. Fellows[1], Sung Kook Chun[1], Natalie Larson[1], Bridget M. Fortin[1], Alisa L. Mahieu[1], Wei A. Song[1], Marcus M. Seldin[1,2], Nicholas R. Pannunzio[1,2,3], Selma Masri[1]*

Diet is a robust entrainment cue that regulates diurnal rhythms of the gut microbiome. We and others have shown that disruption of the circadian clock drives the progression of colorectal cancer (CRC). While certain bacterial species have been suggested to play driver roles in CRC, it is unknown whether the intestinal clock impinges on the microbiome to accelerate CRC pathogenesis. To address this, genetic disruption of the circadian clock, in an *Apc*-driven mouse model of CRC, was used to define the impact on the gut microbiome. When clock disruption is combined with CRC, metagenomic sequencing identified dysregulation of many bacterial genera including *Bacteroides*, *Helicobacter*, and *Megasphaera*. We identify functional changes to microbial pathways including dysregulated nucleic acid, amino acid, and carbohydrate metabolism, as well as disruption of intestinal barrier function. Our findings suggest that clock disruption impinges on microbiota composition and intestinal permeability that may contribute to CRC pathogenesis.

INTRODUCTION

Circadian rhythms are foundational to organismal physiology by consolidating sleep, feeding cycles, as well as metabolic and endocrine cues to a 24-hour period (*1*–*5*). These physiological processes are governed by a cell-autonomous molecular clock driven by the transcription factors CLOCK and BMAL1 (*6*–*9*). Moreover, many important gastrointestinal functions have a circadian rhythm, including intestinal stemness and cell proliferation governed by Wnt signaling (*10*–*15*), immune homeostasis (*16*–*19*), and gut permeability (*20*–*23*). The intestinal clock is of particular interest as altering the timing and content of food can affect host circadian rhythms and the composition of the microbiome (*24*–*29*).

Proper intestinal barrier function is essential for tissue homeostasis as the intestine contains the most abundant and diverse community of symbiotic microorganisms in the body, which influence digestive (*30*–*33*), immune (*34*–*37*), and neural (*38*–*41*) systems. The intestinal microbiota plays an important role in modulating tissue-specific circadian rhythms, and daily fluctuations in bacterial abundance, species, and metabolism have been reported (*25*, *28*, *42*–*45*). Conversely, circadian disruption can also alter microbiome homeostasis, as altering the light-dark cycle shifts the composition and rhythmicity of the microbiota (*46*–*49*), increases gut barrier defects (*20*, *21*), and alters expression of tight junction genes (*20*, *21*, *48*). Aside from environmental alterations, the molecular clock has been directly implicated in controlling microbial rhythms as genetic loss of *Bmal1* or *Per1/2* changed oscillation patterns in microbial abundance (*44*–*46*).

Altering intestinal microbiota composition has important implications for health and disease. Intestinal dysbiosis has been widely reported in pathogenic conditions such as colorectal cancer (CRC) (*50*–*57*). It has been suggested that alterations to microbial abundance and subsequent barrier dysfunction could be a key contributor to early CRC pathogenesis (*52*, *58*–*63*). Bacteria found to be enriched in CRC include *Alistipes*, *Bacteroides*, *Bilophila*, *Coriobacteria*, *Escherichia*, *Fusobacteria*, *Parabacteroides*, and *Prevotella* (*50*, *52*, *55*, *64*–*67*), while *Bifidobacteria*, *Enterobacteria*, *Faecalibacterium*, *Roseburia*, and *Streptococcus* were depleted (*51*, *52*, *64*, *68*). In addition, specific bacteria, including *Fusobacterium nucleatum* (*69*–*72*) and *Bacteroides fragilis* (*73*–*75*), have been reported to play driver roles in CRC pathogenesis by directly modulating Wnt signaling and the activity of c-Myc. Together, these studies suggest that the gut microbiome and intestinal barrier function may play a role in CRC pathogenesis.

Circadian misalignment through night shift work has been implicated as a risk factor for certain cancers (*76*–*86*). Using mouse models of intestinal cancer, we and others have shown that genetic and environmental disruption of the circadian clock promotes CRC progression (*87*–*89*). Therefore, both circadian disruption and gut dysbiosis are key features independently associated with CRC pathogenesis. However, whether the intestinal clock directly impinges on microbial species diversity and abundance during CRC pathogenesis remains fully undefined. To address this, we use metagenomic sequencing to determine cancer-dependent and clock-associated bacteria. We find that certain bacterial species are predominantly cancer associated, including *Fusobacterium mortiferum*, *Parasutterella excrementihominis*, and *Paramuribaculum intestinale*. We also find that *Bacteroides* species including *Bacteroides acidifaciens*, *Bacteroides caecimuri*, and *Bacteroides thetaiotaomicron* are increased upon clock disruption alone or in combination with cancer. Furthermore, we identify alterations in bacterial nucleic acid, amino acid, fatty acid, and carbohydrate metabolic pathways, including those related to mucus degradation, which are associated with reduced mucus staining in colorectal tumors. We also find significant perturbation to intestinal barrier function when the clock is disrupted in the presence of CRC, as we observe dysregulated tight junction and mucin gene expression, and increased permeability to fluorescein isothiocyanate (FITC)–dextran in vitro and in vivo. Overall, our findings indicate that the circadian clock is important for maintaining both intestinal permeability and bacterial homeostasis, and these factors could be important for the pathogenesis of CRC.

[1]Department of Biological Chemistry, University of California Irvine, Irvine, CA 92697, USA. [2]Chao Family Comprehensive Cancer Center, University of California Irvine, Irvine, CA, 92697, USA. [3]Department of Medicine, Division of Hematology/Oncology, University of California Irvine, Irvine, CA 92697, USA.
*Corresponding author. Email: smasri@uci.edu

RESULTS

Clock disruption alters intestinal microbiota composition in a genetic model of CRC

During CRC development, gut dysbiosis and chronic inflammation have been well described for patients (*90*, *91*) and in mouse models (*92*, *93*). It has even been proposed that certain bacteria, such as *F. nucleatum* (*69*–*72*) and *B. fragilis* (*73*–*75*), might have driver roles in CRC progression. Despite findings showing that circadian disruption can alter the intestinal microbiome (*46*–*49*), it is currently unknown how clock mediated changes in bacterial abundance influence CRC pathogenesis. We recently demonstrated that clock disruption accelerated CRC through use of a novel genetically engineered mouse model (GEMM) harboring intestine-specific heterozygous deletion of exons 1 to 15 of the tumor suppressor *Apc* (*Apc*$^{+/\Delta ex1\text{-}15}$ or *Apc*$^{+/-}$) and deletion of exon 8 in both alleles of *Bmal1* (*Bmal1*$^{-/-}$) (Fig. 1A) (*89*). In this GEMM, levels of BMAL1 protein are lost (fig. S1A), and this contributes to disruption of circadian gene expression in the intestine (fig. S1B) (*89*). To identify bacteria that might be involved in clock mediated acceleration of CRC, we performed metagenomic sequencing of feces from wild-type (WT), *Bmal1*$^{-/-}$, *Apc*$^{+/-}$, and *Apc*$^{+/-}$;*Bmal1*$^{-/-}$ mice (Fig. 1A). A significant decrease in species richness was observed between WT and *Apc*$^{+/-}$;*Bmal1*$^{-/-}$ according to both Shannon (Fig. 1B) and Chao (Fig. 1C) α-diversity analyses. Next, we analyzed β-diversity using Bray-Curtis principle covariant analysis to examine overall differences in microbiota composition between groups. WT, *Bmal1*$^{-/-}$, and *Apc*$^{+/-}$ mice were more similar to each other, while the *Apc*$^{+/-}$;*Bmal1*$^{-/-}$ group differed, with its ellipse partially separating from the other genotypes (Fig. 1D). Analysis of similarities (ANOSIM) was performed to test whether the similarity between groups was greater or equal to the similarity within each group. The effect size (R) value was closer to 0 than 1 ($R = 0.173$), indicating that there was a small but significantly ($P = 0.003$) greater difference between groups, relative to within the group (Fig. 1E). Overall,

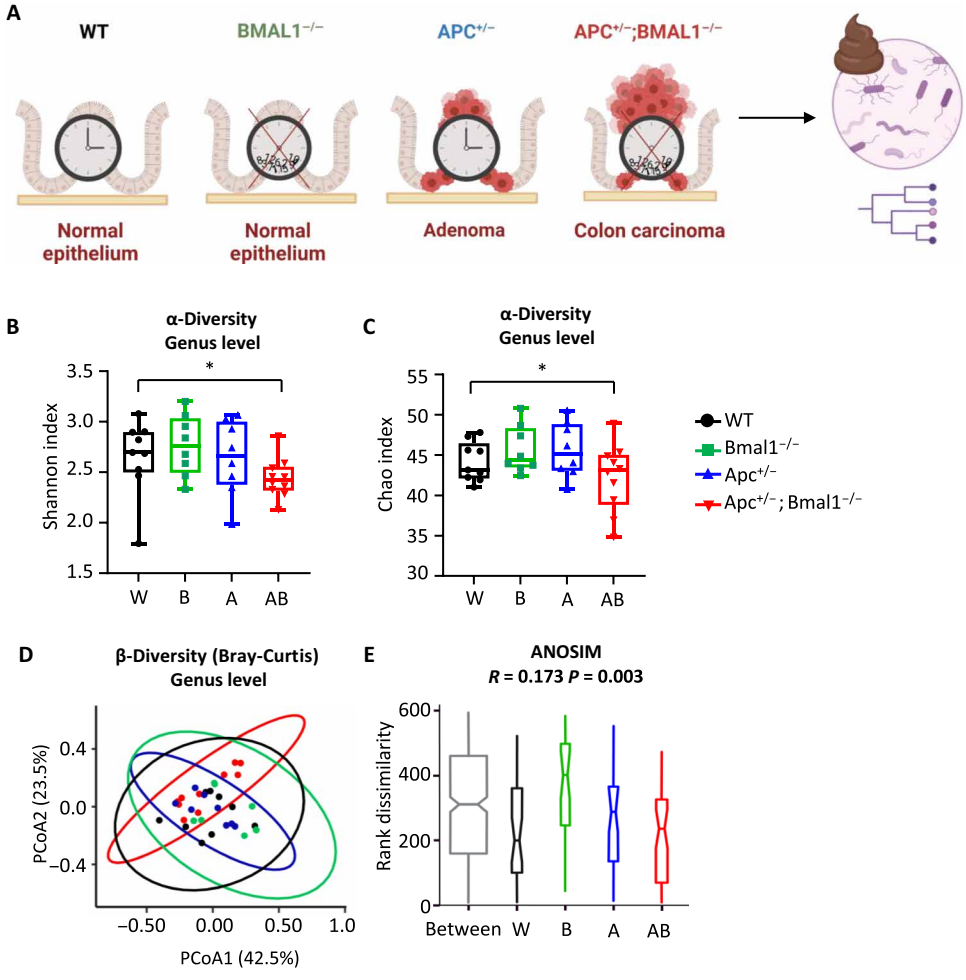

Fig. 1. Clock disruption and cancer alter microbial structure. (**A**) Experimental design of shotgun microbiome sequencing performed on feces from WT, *Bmal1*$^{-/-}$, *Apc*$^{+/-}$, and *Apc*$^{+/-}$;*Bmal1*$^{-/-}$ mice ($n = 9$ for WT, $n = 8$ for *Bmal1*$^{-/-}$ and *Apc*$^{+/-}$, and $n = 10$ for *Apc*$^{+/-}$;*Bmal1*$^{-/-}$ mice). Comparisons of α-diversity in microbiome sequencing at the genus level using Shannon (**B**) and Chao (**C**) indices. Data are expressed as a box plot including the means ± the minimum and maximum values. Statistical significance was determined by the Wilcoxon signed-rank test, and P values from significant multiple comparisons are shown on the graph with * < 0.05. (**D**) β-Diversity as determined by principle covariant analysis (PCoA) using Bray-Curtis distances. Ellipsoids show the 95% confidence region. (**E**) Analysis of similarities (ANOSIM) among genotypes expressed as a box plot. Effect size (R) value indicates the degree of difference between groups (0, no difference; 1, greatest difference), and P value indicates the significance. Genotypes are indicated as follows: WT (W), *Bmal1*$^{-/-}$ (B), *Apc*$^{+/-}$ (A), and *Apc*$^{+/-}$;*Bmal1*$^{-/-}$ (AB).

shifts in microbial composition were found in the clock disrupted tumor-bearing *Apc*$^{+/-}$;*Bmal1*$^{-/-}$ mice.

Bacterial species abundance is altered because of clock disruption and CRC

To investigate which specific bacteria were responsible for the changes to the microbiota community structure, we first examined the abundance of different taxonomic groups. The two most abundant phyla identified were *Firmicutes* and *Bacteroidetes*, with an average abundance across genotypes of 42 and 40%, respectively (Fig. 2A). From WT to single mutants to double mutant, there was a sequential reduction in average *Firmicutes* and a sequential increase in average *Bacteroidetes* abundances (Fig. 2A). Bacterial species were further classified on the basis of alterations in the clock mutant mice, tumor-bearing animals, or in both groups relative to WT (Fig. 2, B to D). MaAsLin2 (microbiome multivariable associations with linear models) analysis was performed to preserve statistical power while controlling for false discovery, an essential consideration in meta-omics data analysis (*94*). Clock-associated bacteria included *B. acidifaciens*, *B. caecimuris*, and *Bacteroides congonensis*, which significantly increased in *Apc*$^{+/-}$;*Bmal1*$^{-/-}$ and showed a non-statistically significant increase in *Bmal1*$^{-/-}$ mice (Fig. 2B). Another clock-dependent bacterium was *Helicobacter apodemus*, which significantly increased

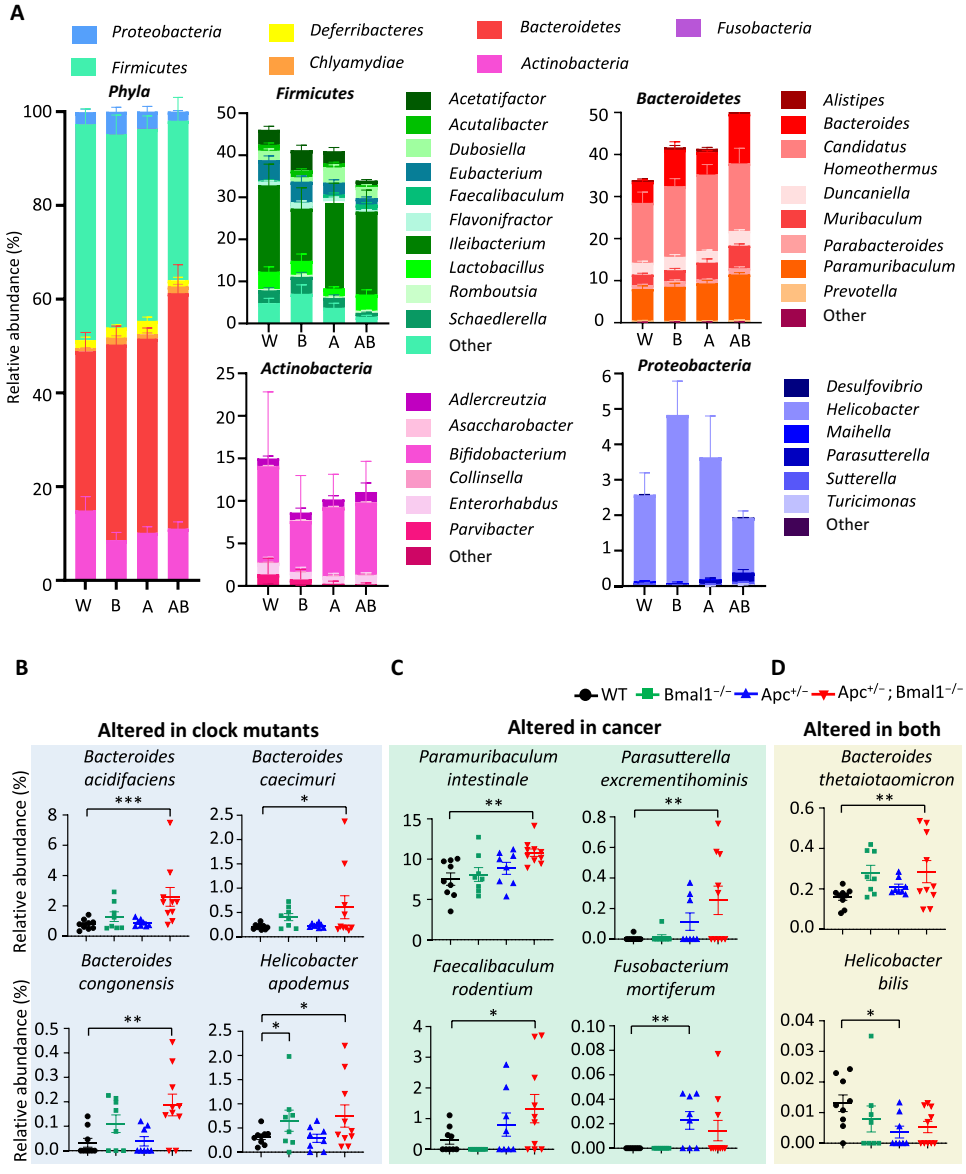

Fig. 2. Clock disruption and CRC alter microbiome composition. (**A**) Relative abundance of microbial phyla and genera between WT, *Bmal1*$^{-/-}$, *Apc*$^{+/-}$, and *Apc*$^{+/-}$;*Bmal1*$^{-/-}$ mice ($n = 9$ for WT, $n = 8$ for *Bmal1*$^{-/-}$ and *Apc*$^{+/-}$, and $n = 10$ for *Apc*$^{+/-}$;*Bmal1*$^{-/-}$ mice). Genotypes are indicated as follows: WT (W), *Bmal1*$^{-/-}$ (B), *Apc*$^{+/-}$ (A), and *Apc*$^{+/-}$;*Bmal1*$^{-/-}$ (AB). Relative abundance of bacteria altered in fecal samples from clock mutants (**B**), cancer mutants (**C**), and in both clock and cancer mutants (**D**). Error bars represent SEM, significance was determined using MaAsLin2, and *P* values of pathways with significant *q* values ($q > 0.25$) are shown on the graph with * < 0.05, ** < 0.01, and *** < 0.001.

in both *Bmal1*$^{-/-}$ and *Apc*$^{+/-}$;*Bmal1*$^{-/-}$ (Fig. 2B). CRC-associated bacteria were identified as *P. intestinale*, *P. excrementihominis*, and *Faecalibaculum rodentium*, which were significantly increased in *Apc*$^{+/-}$;*Bmal1*$^{-/-}$ mice with a nonsignificant increase in *Apc*$^{+/-}$, while *F. mortiferum* was significantly increased only in *Apc*$^{+/-}$ mice (Fig. 2C). Last, bacterial species altered in both clock mutant and CRC mice were identified (Fig. 2D). *Helicobacter bilis* decreased in all mutant mice relative to WT, which was significant for *Apc*$^{+/-}$ mice. *B. thetaiotaomicron* significantly increased in *Apc*$^{+/-}$;*Bmal1*$^{-/-}$ and showed nonsignificant increases in *Bmal1*$^{-/-}$ and *Apc*$^{+/-}$ mice (Fig. 2D). Together, these data classify bacterial species to be associated with intestinal clock disruption, tumor progression, or a combination of both.

Identification of bacterial biomarker species

Linear discriminant analysis effect size (LEfSe) analysis was performed to identify key bacterial biomarker species that significantly contribute to the overall microbial phenotype (*95*). Cladograms demonstrate the relationships between taxonomic levels, spanning from kingdom in the center to species on the outside of the circle (Fig. 3). Blocks of color on the figure indicate where a significant difference has been identified at the order, family, genus, or species level. Purple, green, blue, and red circles within the cladograms reflect significant differences in WT, *Bmal1*$^{-/-}$, *Apc*$^{+/-}$, or *Apc*$^{+/-}$;*Bmal1*$^{-/-}$, respectively. Bacterial biomarker species ordered by the linear discriminant analysis (LDA) score, which describes the degree of difference between groups, are shown in fig. S2. WT–versus–single mutant comparisons were performed to investigate the contribution of *Bmal1* or *Apc* deletion alone (Fig. 3, A and B, and fig. S2, A and B). *B. caecimuri* (e) and *H. apodemus* (b4) were associated with *Bmal1*$^{-/-}$ microbiomes, while *Collinsella intestinalis* (b), *Faecalibacterium rodentium* (b1), and *Sutterella wadsworthensis* (b3) were associated with WT microbiomes (Fig. 3A and fig. S2A). *F. mortiferum* (b2) was only linked to CRC in *Apc*$^{+/-}$ mice (Fig. 3B and fig. S2B). Similar to the MaAsLin2 analysis (Fig. 2D), *B. thetaiotaomicron* (h) was associated with both *Bmal1*$^{-/-}$ and *Apc*$^{+/-}$ mice (Fig. 3, A and B, and S2, A and B). These species biomarker data support our prior observations that *Bacteroides* and *Helicobacter* species are influenced by circadian clock disruption, while *Fusobacteria* are altered in CRC development (Fig. 2, B to D).

When *Bmal1*$^{-/-}$ versus *Apc*$^{+/-}$;*Bmal1*$^{-/-}$ microbiomes were compared, many more bacteria from diverse phyla were identified (Fig. 3C and fig. S2C). *Firmicutes* were largely more associated with the nontumor microbiomes of *Bmal1*$^{-/-}$ (Fig. 3C and fig. S2C) or WT mice (fig. S2E). Key *Apc*$^{+/-}$;*Bmal1*$^{-/-}$-associated bacteria, according to the highest LDA score, were *Muribaculum intestinale* (j) and *P. intestinale* (k) (Fig. 3C and fig. S2C). *Apc*$^{+/-}$ versus *Apc*$^{+/-}$;*Bmal1*$^{-/-}$ microbiomes were compared, and the entire family *Bacteroidaceae* was strongly associated with *Apc*$^{+/-}$;*Bmal1*$^{-/-}$ rather than *Apc*$^{+/-}$ (Fig. 3D and S2D). Many bacteria enriched in *Apc*$^{+/-}$ were also enriched in WT or *Bmal1*$^{-/-}$ mice such as *Lactonifactor longoviformis* (q), *Extibacter muris* (y), *Roseburia hominis* (a1), and *Helicobacter typhlonius* (b7) (Fig. 3, C and D, and fig. S2, C to E). This suggests that these bacteria are only down-regulated when clock disruption and CRC are combined. Conversely, *Megasphaera elsdenii* (r) and *Bacteroides stercoris* (g) were associated with the clock-driven adenocarcinoma state of *Apc*$^{+/-}$;*Bmal1*$^{-/-}$ when compared to WT, *Bmal1*$^{-/-}$, or *Apc*$^{+/-}$ microbiomes (Fig. 3, C and D, and fig. S2, C to E). *M. elsdenii* is a lactate-utilizing bacterium and thus could be associated with more advanced CRC where tumor-derived lactate is at high concentrations in the intestinal epithelium (*96*). Overall, *Bacteroides*, *Helicobacter*, and *Fusobacterium* species are altered upon clock disruption or CRC, but the combination of these mutations results in more substantial bacterial changes arising from a broad spectrum of taxonomic groups.

Identification of altered metabolic pathways upon clock disruption and CRC

Previous studies have suggested that, despite high interindividual variability in microbial species, the functional output of the microbiota remains relatively conserved (*97*). As metagenomic sequencing identifies many bacterial genes, rather than just the 16*S* gene, we used HUMAnN 3.0 to directly attribute bacterial gene sequences to altered functional pathways (*98*). The most abundant pathways across groups included uridine 5′-monophosphate biosynthesis, transfer RNA charging, folate transformations, and sucrose and valine biosynthesis, reflecting the major metabolic functions of the microbiota (fig. S3). The top 50 significantly altered pathways, as determined by MaAsLin2 (*94*), are shown in Fig. 4A. The six pathways that were the most altered in *Apc*$^{+/-}$;*Bmal1*$^{-/-}$ microbiomes were amino acid (methionine and Pre-Q0), vitamin (folate), carbohydrate (anhydromuro-peptide and peptidoglycan), and nucleic acid (purine) metabolism (Fig. 4B and fig. S4A). The L-methionine, folate, and purine nucleotide metabolic pathways were also increased significantly in *Apc*$^{+/-}$ microbiomes (Fig. 4B and fig. S4A). Many pathways involving nucleic acid metabolism were up-regulated in the tumor-bearing *Apc*$^{+/-}$ and *Apc*$^{+/-}$;*Bmal1*$^{-/-}$ microbial gene sequences (Fig. 4A). Furthermore, multiple fatty acid metabolic pathways were increased in *Apc*$^{+/-}$ microbiomes, including fatty acid elongation and 8-amino-7-oxononanoate biosynthesis, while amino acid metabolic pathways such as arginine biosynthesis and queuosine biosynthesis were up-regulated in *Apc*$^{+/-}$;*Bmal1*$^{-/-}$ microbiomes (Fig. 4A). Of the top six pathways increased in *Apc*$^{+/-}$;*Bmal1*$^{-/-}$ microbiomes, the carbohydrate metabolism–related anhydromuro-peptide recycling and peptidoglycan maturation pathways were also significantly increased in *Bmal1*$^{-/-}$ microbiomes (fig. S4A). We identified five other pathways that increased in *Bmal1*$^{-/-}$ and *Apc*$^{+/-}$;*Bmal1*$^{-/-}$ microbiomes, suggesting that they are associated with circadian disruption (fig. S4B). These involved homolactic fermentation, thiamine metabolism, phospholipid biosynthesis, and purine nucleobases degradation.

The six most down-regulated pathways in *Apc*$^{+/-}$;*Bmal1*$^{-/-}$ microbiomes involved carbohydrate (stachyose, glucose, hexuronide/hexuronate, and cytidine 5′-monophosphate legionaminate), energy (anaerobic), and vitamin (biotin) metabolism (Fig. 4, A and C, and fig. S4C). The notable down-regulation of hexuronide and hexuronate degradation pathways in our *Apc*$^{+/-}$;*Bmal1*$^{-/-}$ mice (Fig. 4C) suggested alterations in carbohydrate metabolism. Additional pathways involving degradation of hexuronides and hexuronates were significantly down-regulated in *Apc*$^{+/-}$;*Bmal1*$^{-/-}$ microbiomes including D-galacturonate, D-fructuronate, and β-D-glucuronosides (comprising glucuronate and fructuronate) (fig. S4D). Pathways involving galactose degradation were also reduced in *Bmal1*$^{-/-}$ and *Apc*$^{+/-}$;*Bmal1*$^{-/-}$ microbiomes (fig. S4, D and E), and galactose is a key residue of mucin *O*-glycans (*99*, *100*). This suggests a down-regulation of dietary and host-derived carbohydrate degradation pathways, including mucus-derived sugars, in *Apc*$^{+/-}$;*Bmal1*$^{-/-}$ microbiomes. In summary, we found that either clock disruption or CRC development altered many different bacterial metabolic

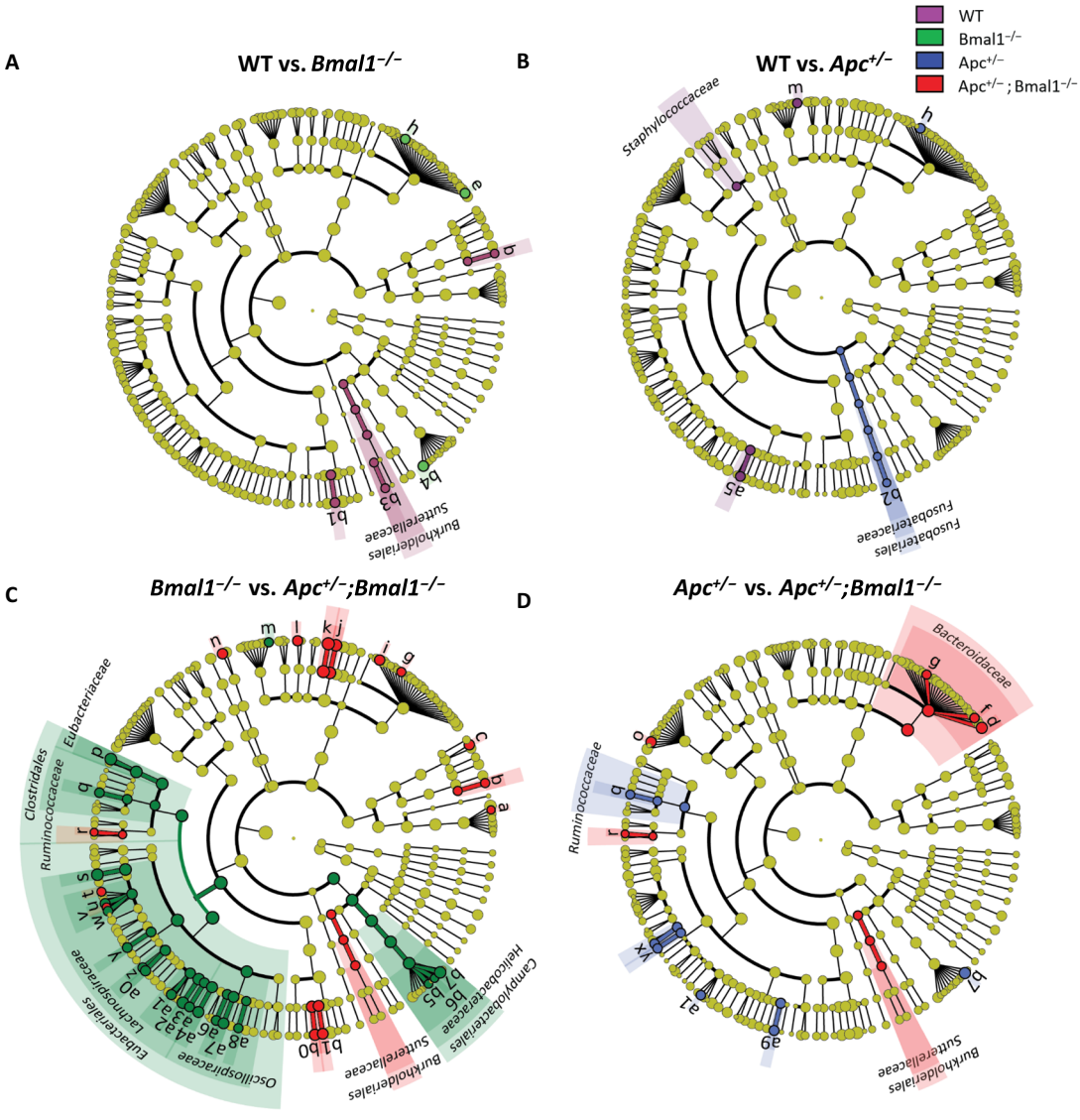

Actinobacteria

a *Bifidobacterium gallinarum*
b *Collinsella intestinalis*
c *Enterorhabdus musicola*

Bacteroidetes

d *Bacteroides acidifaciens*
e *Bacteroides caecimuri*
f *Bacteroides congonensis*
g *Bacteroides stercoris*
h *Bacteroides thetaiotaomicron*
i *Bacteroides vulgatus*
j *Muribaculum intestinale*
k *Paramuribaculum intestinale*
l *Prevotella copri*

Firmicutes

m *Parabacteroides chinchillae*
n *Chylamydia muridarum*
o *Lactobacillus reuteri*
p *Eubacterium plexicaudatum*
q *Lactonifactor longoviformis*
r *Megasphaera elsdenii*
s *Acetatifactor muris*
t *Blautia hansenii*
u *Blautia schinkii*
v *Blautia wexlerae*
w *Ruminococcus gnavus*
x *Enterocloster lavalensis*
y *Extibacter muris*
z *Lachnoclostridium phocaeense*
a0 *Chlostridium scindens*
a1 *Roseburia hominis*
a2 *Schaedlerella arabinosiphila*
a3 *Tyzzerella nexilis*
a4 *Acutalibacter muris*
a5 *Agathobaculum desmolans*
a6 *Angelakisella massiliensis*
a7 *Flavonifractor plautii*
a8 *Clostridium methylpentosum*
a9 *Pseudoflavonifractor capillosus*
b0 *Dubosiella newyorkensis*
b1 *Faecalibacterium rodentium*

Fusobacteria

b2 *Fusobacterium mortiferum*

Proteobacteria

b3 *Sutterella wadsworthensis*
b4 *Helicobacter apodemus*
b5 *Helicobacter hepaticus*
b6 *Helicobacter magdeburgensis*
b7 *Helicobacter typhlonius*

Fig. 3. Clock disruption and CRC alter microbiome biomarker species. Linear discriminant analysis effect size (LEfSe) of microbiome sequencing data from all four genotypes ($n = 9$ for WT, $n = 8$ for *Bmal1*$^{-/-}$ and *Apc*$^{+/-}$, and $n = 10$ for *Apc*$^{+/-}$;*Bmal1*$^{-/-}$ mice). Cladograms show comparisons between WT and *Bmal1*$^{-/-}$ (**A**), WT and *Apc*$^{+/-}$ (**B**), *Bmal1*$^{-/-}$ and *Apc*$^{+/-}$;*Bmal1*$^{-/-}$ (**C**), and *Apc*$^{+/-}$ and *Apc*$^{+/-}$;*Bmal1*$^{-/-}$ (**D**). Bacterial species corresponding to each letter are shown in the key below, grouped by phylum. Blocks of purple (WT), green (*Bmal1*$^{-/-}$), blue (*Apc*$^{+/-}$), or red (*Apc*$^{+/-}$;*Bmal1*$^{-/-}$) in the figure show a significant enrichment in the microbiota of that genotype has been identified at the order, family, genus, or species level. Circles in the same colors reflect where there is a significant difference at the genus or species level. Species are indicated by an alphanumeric key with full species names below the diagrams, grouped by phylum.

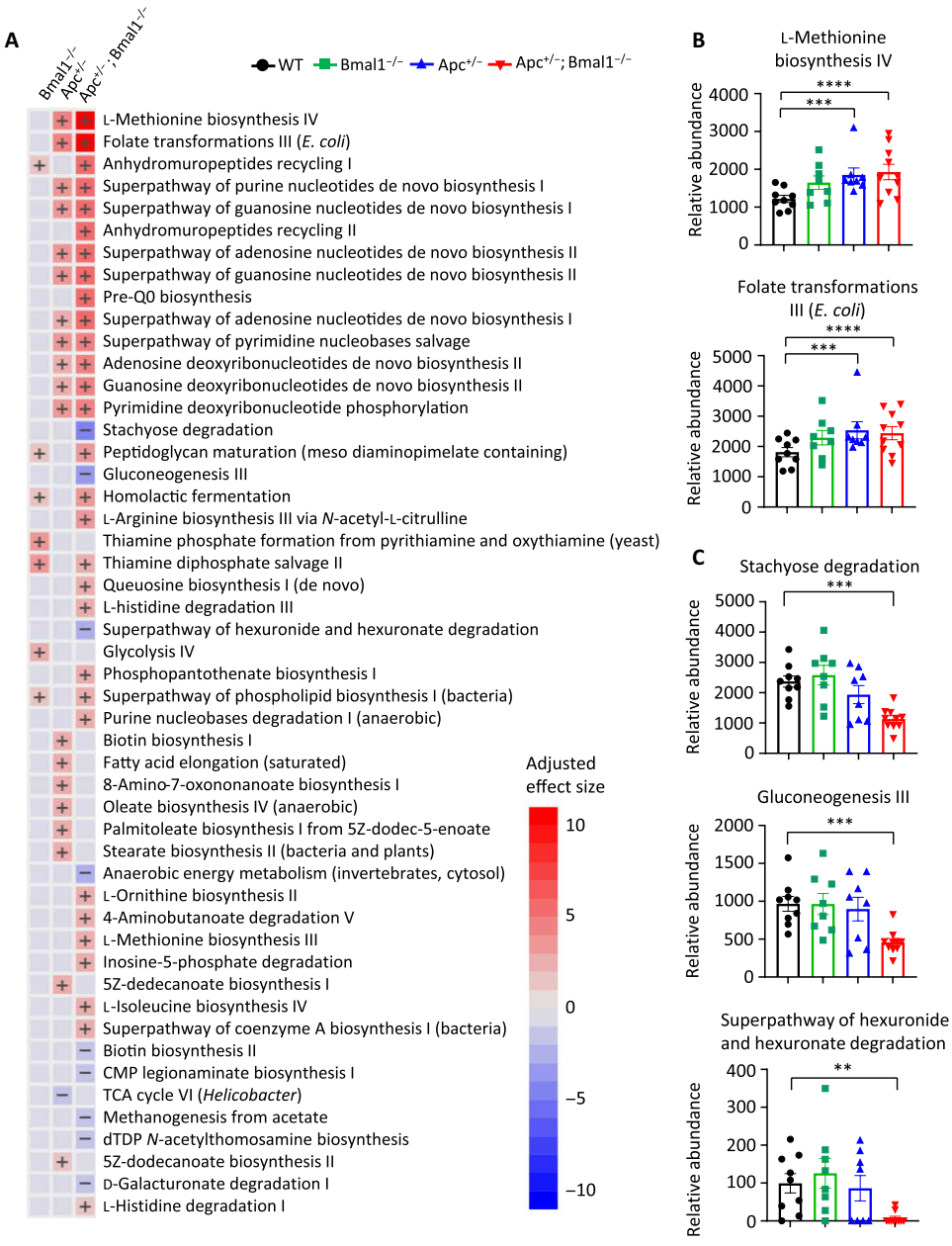

Fig. 4. Microbial pathway analysis in clock disrupted and tumor-bearing mice. Microbial functional pathways were profiled with HUMAnN using microbiome sequencing data from all four genotypes ($n = 9$ for WT, $n = 8$ for *Bmal1*$^{-/-}$ and *Apc*$^{+/-}$, and $n = 10$ for *Apc*$^{+/-}$;*Bmal1*$^{-/-}$ mice). (**A**) Significant changes as determined by MaAsLin2 of microbial pathways altered in *Bmal1*$^{-/-}$, *Apc*$^{+/-}$, and *Apc*$^{+/-}$;*Bmal1*$^{-/-}$ mice relative to WT. Pathways are colored by effect size adjusted by *q* value, with signs indicating the direction of change. Relative abundance in all genotypes of the top pathways most increased (**B**) or decreased (**C**) in *Apc*$^{+/-}$;*Bmal1*$^{-/-}$ relative to WT. Additional pathways are shown in fig. S4 (A and B). Error bars represent SEM, significance was determined using MaAsLin2, and *P* values of pathways with significant *q* values ($q > 0.25$) are shown on the graph with ** < 0.01, *** < 0.001, and **** < 0.0001.

pathways, with activation of nucleic, amino and fatty acid–related pathways, and a decrease in carbohydrate and energy metabolism.

Host mucus metabolism is altered by circadian disruption and tumorigenesis

Among carbohydrate metabolic pathways that were identified (Fig. 4 and fig. S3), many involved the degradation of sugars, such as hexuronides, that are found in dietary nutrients and mucus (*99*). As dietary composition and food intake were unchanged in these mice (*45*, *89*), alterations to downstream bacterial carbohydrate metabolic pathways could result from changes due to host mucus production. This is of particular interest as the mucus layer forms a key part of the epithelial barrier that enables absorption of nutrients while preventing translocation of bacteria into the sterile submucosa and blood (*101*, *102*) and increased intestinal and systemic inflammation (*103*). We therefore examined our previously published RNA sequencing (RNA-seq) data

(*89*) for changes in the expression of genes related to mucus production in our four genotypes. We found that expression of the four most highly expressed mucin genes—*Muc2*, *Muc3*, *Muc3a*, and *Muc13* (Fig. 5A), as well as the secretory and goblet cell markers *Atoh1*, *Clca1*, and *Fcgbp* (fig. S1C), was significantly decreased in organoids isolated from the intestinal epithelium of $Apc^{+/-}$;$Bmal1^{-/-}$ mice.

As mucus thickness is known to be circadian (*42*, *104*), mucin-related gene expression was profiled over the circadian cycle from intestinal epithelial cells (IECs) from WT mice. We confirmed that there was a significant circadian rhythm in *Bmal1*, *Cry2*, *Dbp*, and *Reverb*-α gene expression in IECs, with period values close to 24 (fig. S5A and table S2). We then investigated the rhythmic expression

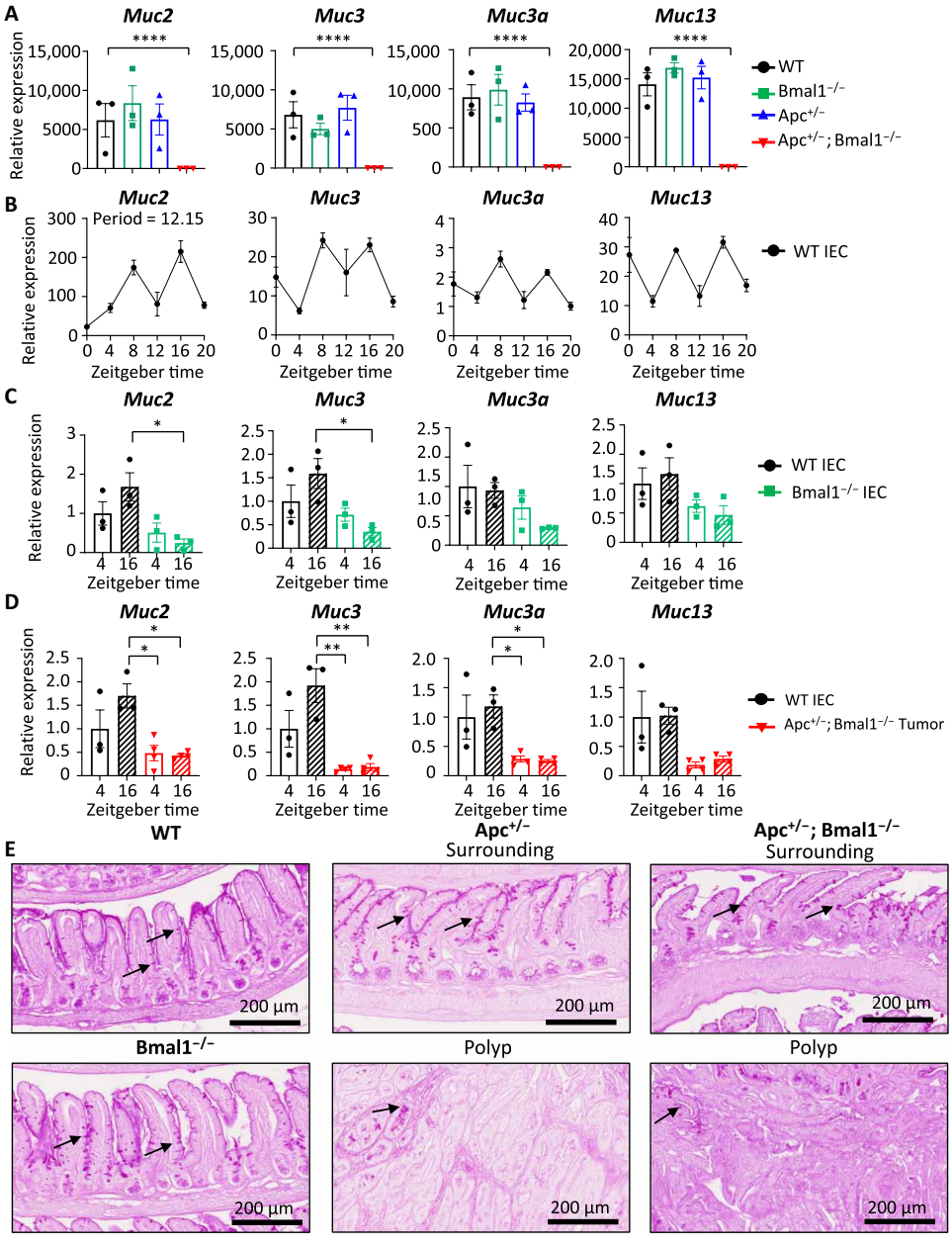

Fig. 5. Mucin gene expression and mucus levels are reduced in CRC. (**A**) Expression of the top four most highly expressed mucin genes as determined by RNA sequencing (RNA-seq) of small intestinal organoids from all four genotypes ($n = 3$ organoid lines derived from independent mice). (**B**) Expression of mucin genes in IECs from WT mice relative to zeitgeber time, as determined by quantitative polymerase chain reaction (qPCR; $n = 5$ independent mice per time point). Average circadian period is shown when the rhythmicity *P* value was less than 0.01. All values are shown in table S2. (**C**) Expression of mucin genes in WT and $Bmal1^{-/-}$ IECs collected from $n = 3$ independent mice at ZT4 and ZT16. (**D**) Expression of mucin genes in WT IECs and $Apc^{+/-}$;$Bmal1^{-/-}$ tumors collected from $n = 3$ independent mice at ZT4 and ZT16. (**E**) Periodic acid–Schiff (PAS) staining on formalin-fixed paraffin-embedded small intestinal sections from WT, $Bmal1^{-/-}$, $Apc^{+/-}$, and $Apc^{+/-}$;$Bmal1^{-/-}$ mice. Tumor-bearing genotypes are divided into predominantly normal (surrounding) or predominantly tumor containing (polyp) areas. Scale bars, 200 µm. Error bars represent SEM, and statistical significance was determined by DEseq2 for (A) and by one-way analysis of variance (ANOVA) with Tukey's multiple comparisons for (C) and (D). Asterisks represent false discovery rate (FDR) or *P* values from multiple comparisons with * < 0.05, ** < 0.01, and **** < 0.0001. Comparisons without labels are not significant.

of the four most expressed mucin genes according to our RNA-seq data. We found that, while *Muc2* was significantly rhythmic, the other mucin genes did not display a clear circadian rhythm (Fig. 5B and table S2). A previous study found that *Muc2* is not rhythmic in conventional or germ free mice (*105*); however, another report identified that intestine-specific *Bmal1* loss ablated *Muc2* rhythmicity (*45*). Therefore, to determine whether genetic disruption of the circadian clock affects mucin gene expression, IECs were isolated from WT and $Bmal1^{-/-}$ mice at two different times of day. Core clock and clock-controlled genes were altered in $Bmal1^{-/-}$ IECs versus WT, as expected (fig. S5C). Consistent with Fig. 5B, no significant difference in expression in WT IECs between zeitgeber time 4 (ZT4) and ZT16 was observed in mucin gene expression (Fig. 5C). However, the expression of *Muc2* and *Muc3* was significantly dampened in IECs isolated from $Bmal1^{-/-}$ mice at ZT16 (Fig. 5C). With the exception of *Muc2*, many mucin genes are not dynamically rhythmic in vivo. However, the expression of *Muc2* and *Muc3* is affected by genetic disruption of the circadian clock, suggesting a complex regulatory axis that could affect intestinal mucus turnover.

MaAsLin2 pathway analysis identified alterations in carbohydrate metabolism that likely affect mucus and intestinal barrier pathways (Fig. 4). To define whether mucus levels are altered in colorectal tumors, mucin gene expression analysis was performed at two time points from either WT IECs or $Apc^{+/-}$;$Bmal1^{-/-}$ tumors. A significant reduction in the expression of multiple clock genes was observed (fig. S5E). This is consistent with reports that core clock genes are misregulated in CRC (*13*, *106*–*110*). Mucin gene expression was down-regulated in $Apc^{+/-}$;$Bmal1^{-/-}$ tumors (Fig. 5D), which corresponded to the loss of tumor-specific clock gene expression (fig. S5E). To determine whether changes to mucin expression resulted in functional alterations in mucus levels, periodic acid–Schiff (PAS) staining was performed to quantify carbohydrates as PAS oxidizes and colors sugars found in glycoproteins and mucins. In particular, we wanted to define whether mucus levels are clock or tumor dependent. High-magnification images with black arrows indicating goblet cells are shown in Fig. 5E, while lower-magnification images of biological replicates are in fig. S6A. We found no differences in PAS staining between WT and $Bmal1^{-/-}$ either qualitatively by looking at the glycocalyx layer, in goblet cell numbers (Fig. 5E and fig. S6A), or by quantifying PAS staining relative to epithelial area (fig. S6B). However, we found that mucus staining was decreased in the tumors of $Apc^{+/-}$ and $Apc^{+/-}$;$Bmal1^{-/-}$ mice with a complete loss of goblet cells in large areas of the tumor (Fig. 5E and fig. S6, A and B). Collectively, we found altered intestinal expression of mucins upon genetic clock disruption and cancer; however, PAS staining identified a reduction in mucus levels only in advanced tumor regions.

The intestinal clock governs expression of tight junction genes

While mucus production is a key part of barrier function, an additional essential aspect of intestinal integrity is the tight junctions that join epithelial cells, mediate paracellular permeability, and prevent bacteria from invading underlying tissues (*111*, *112*). RNA-seq data were interrogated to identify expression changes in tight junction genes upon clock disruption and CRC pathogenesis (*89*). A significant increase in *Cldn4* and *Tjp1* (ZO-1) expression was found, with a significant decrease in *Cldn7*, *Cldn15*, *Cldn23*, and *Ocln* in $Apc^{+/-}$;$Bmal1^{-/-}$ organoids relative to WT (Fig. 6A and fig. S1D). *Cldn8* expression was significantly increased in $Bmal1^{-/-}$ organoids (Fig. 6A), with a similar trend in $Apc^{+/-}$;$Bmal1^{-/-}$ organoids, suggesting that it might be regulated by the circadian clock.

Previous studies have found that the expression of certain tight junction genes such as *Cldn1*, *Cldn3*, and *Ocln* exhibits time-of-day–dependent differences in the intestine (*20*, *113*, *114*), with additional rhythmic genes including *Cldn2*, *Cldn4*, and *Cldn5* identified in other tissues such as the kidney and liver (*115*–*117*). Therefore, expression analysis for tight junction genes was performed in WT IECs over the circadian cycle. *Cldn8* showed significant circadian oscillations in gene expression in IECs over the circadian day/night cycle (Fig. 6B and table S2), while other genes were not significantly rhythmic (Fig. 6B, fig. S5B, and table S2). To determine whether these gene expression changes were also *Bmal1* dependent, quantitative polymerase chain reaction (qPCR) was performed for tight junction genes using WT and $Bmal1^{-/-}$ IECs collected at two different times. *Cldn8* was significantly up-regulated upon loss of *Bmal1*, and *Tjp1* decreased, while changes to other tight junction genes were less apparent (Fig. 6C and fig. S5D). To determine whether tight junction gene expression was altered in tumors, we used WT IECs and $Apc^{+/-}$;$Bmal1^{-/-}$ tumor samples at two circadian time points. A significant reduction in tight junction gene expression was observed for *Ocln* and *Tjp1*, with dampening for *Cldn7* and *Cldn8* in tumor samples (Fig. 6D and fig. S5E). Together, our data indicate that genetic clock disruption alone has a modest impact on expression of tight junction genes, but this is exacerbated in the context of advanced CRC.

Clock-dependent control of intestinal barrier function

It has been reported that intestinal permeability oscillates over the day-night cycle (*25*). However, the contribution of clock disruption on intestinal permeability during tumor progression remains unknown. To test this, an in vitro intestinal epithelial model using human Caco-2 cells was used to establish differentiated monolayers for permeability assays (*118*). We chose 12-hour intervals so that we could capture the entire 24-hour circadian cycle with two time points and thus be able to compare gene expression to permeability. We synchronized Caco-2 cells in culture and, as expected, found that the expression of *BMAL1* and *REVERBα* was significantly higher at 24 hours relative to 12 hours after synchronization (Fig. 7A). We then examined mucin genes and found that there was a significant difference in *MUC2* and *MUC17* (orthologous to mouse *Muc3*) but no difference in *MUC3A* and *MUC13* between circadian time 12 (CT12) and CT24 (Fig. 7B). We also examined tight junction genes and observed significant decreases in *CLDN2*, *CLDN4*, and *CLDN7*; significant increases in *CLDN8* and *OCLN*; and no change in *TJP1* (Fig. 7C). On the basis of these changes in gene expression, we tested the permeability of Caco-2 epithelial monolayers grown on transwell supports to 4-kDa FITC-dextran at 12- and 24-hours after synchronization. We observed a time-dependent control in FITC-dextran permeability in the Caco-2 monolayer (Fig. 7D). This was inversely correlated with *BMAL1*, *REVERBα*, *CLDN8*, and *OCLN* expression, in that lower expression correlated with higher permeability.

Our data suggest that there is a time-dependent correlation between tight junction and mucin gene expression, and intestinal permeability. Therefore, to investigate intestinal permeability in vivo, we leveraged our GEMM to determine whether the circadian clock regulates intestinal barrier function alone or in the context of CRC. Fasted mice were gavaged with 4-kDa FITC-dextran at ZT23, and serum fluorescence was measured at ZT0 as a readout

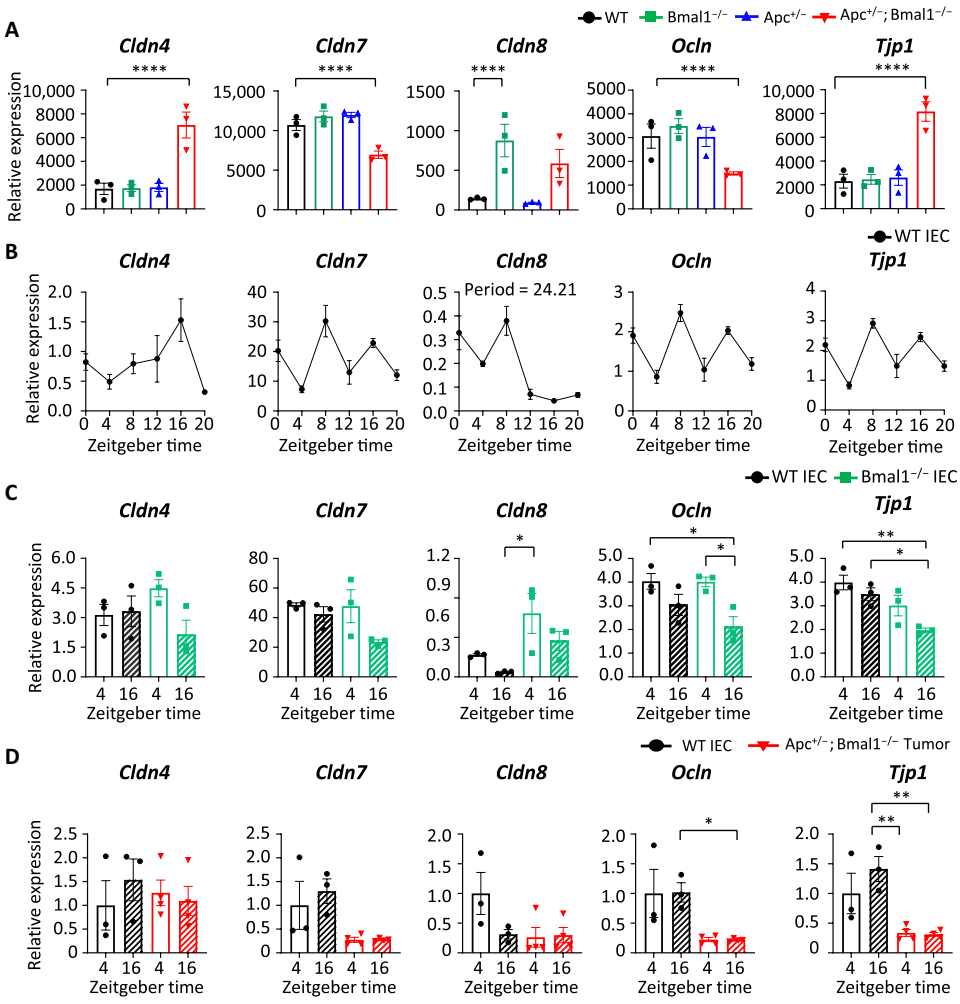

Fig. 6. Tight junction gene expression is clock dependent and disrupted in CRC. (**A**) Expression of five key tight junction genes as determined by RNA-seq of small intestinal organoids from all four genotypes ($n = 3$ organoid lines derived from independent mice). (**B**) Expression of tight junction genes in IECs from WT mice relative to zeitgeber time, as determined by qPCR (n = 5 independent mice per time point). Average circadian period is shown when the rhythmicity P value was less than 0.01. All values are shown in table S2. (**C**) Expression of tight junction genes in WT and *Bmal1*$^{-/-}$ IECs collected from $n = 3$ independent mice at ZT4 and ZT16. (**D**) Expression of tight junction genes in WT IECs and *Apc*$^{+/-}$;*Bmal1*$^{-/-}$ tumors collected from $n = 3$ independent mice at ZT4 and ZT16. Error bars represent SEM, and statistical significance was determined by DEseq2 for (A) and by one-way ANOVA with Tukey's multiple comparisons for (C) and (D). Asterisks represent FDR or P values from multiple comparisons with * < 0.05, ** < 0.01, and **** < 0.0001. Comparisons without labels are not significant.

for intestinal permeability. ZT0 was chosen on the basis of published findings that illustrated a peak in gut barrier function (*25*), as we wanted to select the time when permeability was lowest in WT mice. As shown in Fig. 7E, the single-mutant *Bmal1*$^{-/-}$ and *Apc*$^{+/-}$ mice displayed a nonsignificant increase in intestinal permeability. However, there was a significant increase in intestinal permeability in the double-mutant *Apc*$^{+/-}$;*Bmal1*$^{-/-}$ mice (Fig. 7E). This suggests that clock disruption and CRC progression together exacerbate intestinal barrier function. Together, our data demonstrate that clock disruption and CRC development shift microbiome composition, with altered abundance of bacteria such as *Bacteroides*, *Helicobacter*, and *Megasphaera* and changes in a wide range of microbial metabolites. These bacterial changes, accompanied by reduced tumor mucus staining, altered tight junction gene expression, and defective intestinal barrier function, could exacerbate CRC progression.

DISCUSSION

We leveraged our GEMM of clock disruption and CRC to define alterations in the gut microbiome using metagenomic sequencing. We identified bacterial species that are increased upon *Bmal1* loss, including *B. caecimuri* and *H. apodemus*, and bacteria that are increased in an *Apc*-driven model of CRC, such as *F. mortiferum* (Figs. 2 and 3). Substantial shifts in microbiome composition were found when clock disruption and CRC were combined, with greater changes in *Bacteroides* species and identification of additional species such as *M. elsdenii* (Figs. 1 to 3). Functionally, we found increases in many bacterial pathways related to nucleic, amino, and fatty acid metabolism in CRC mice, while many carbohydrate degradation pathways, including dietary and mucus-related sugars, were reduced in *Apc*$^{+/-}$;*Bmal1*$^{-/-}$ microbiomes (Fig. 4). This could be linked to a reduction in host mucus, as we identified less mucus staining in advanced tumors (Fig. 5). We also observed rhythmic

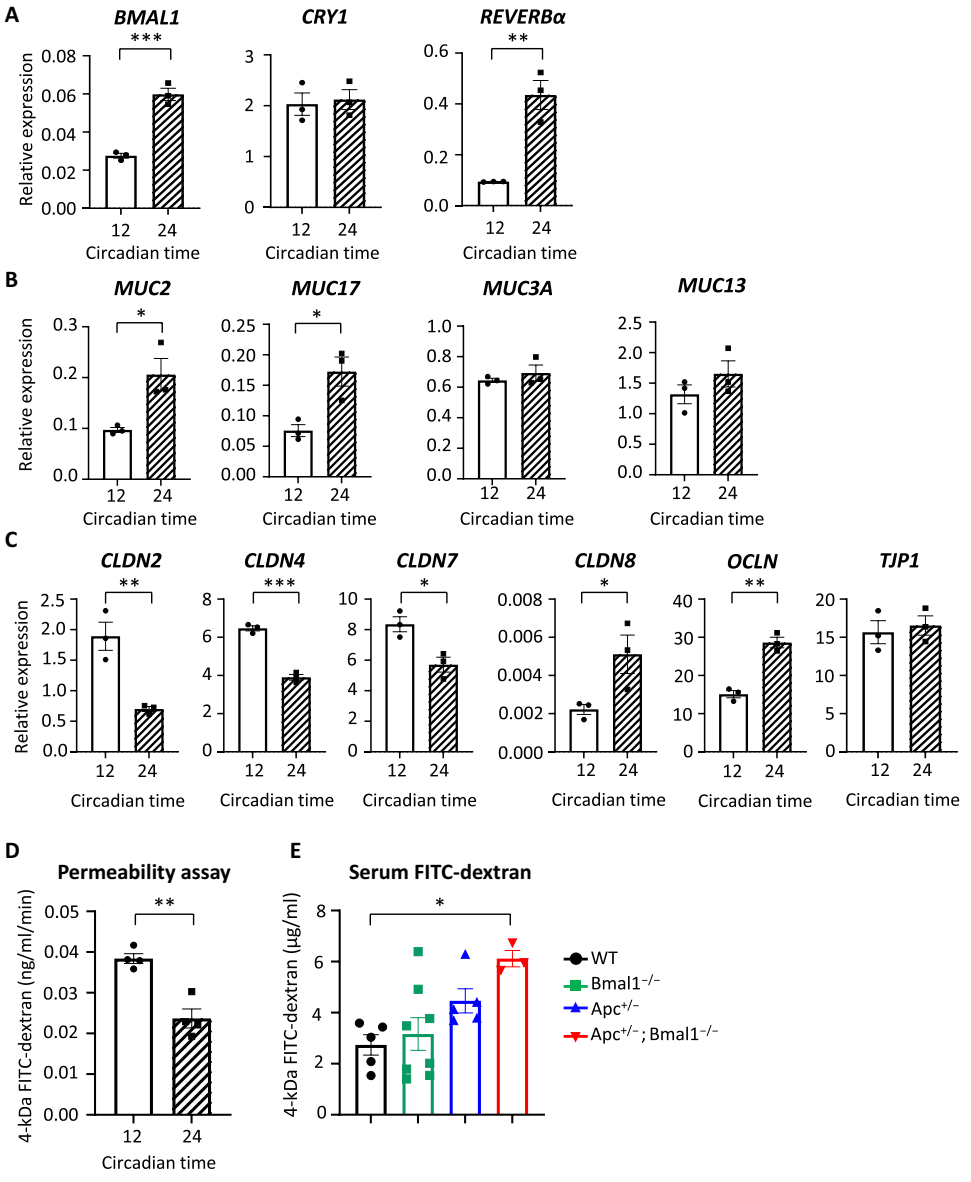

Fig. 7. Cell monolayer permeability is clock dependent, and intestinal barrier function is reduced when clock dysregulation and CRC are combined. Expression of core clock (**A**), mucin (**B**), and tight junction (**C**) genes in DEX synchronized Caco-2 cells ($n = 3$ independent experiments). (**D**) Monolayer permeability of DEX synchronized Caco-2 cells as determined by 4-kDa FITC-dextran transfer in a transwell assay ($n = 3$ independent experiments). (**E**) Intestinal permeability from WT, *Bmal1*, $Apc^{+/-}$, and $Apc^{+/-}$;$Bmal1^{-/-}$ mice as determined by gavage of 4-kDa FITC-dextran (600 mg/kg) at ZT23 and serum collection at ZT0 ($n = 3$ to 8 independent mice). Statistical significance was determined by Student's unpaired *t* test for (A) to (D) and by one-way ANOVA with Tukey's multiple comparisons for (E). Asterisks represent *P* values from unpaired t-test or multiple comparisons with * < 0.05, ** < 0.01, and *** < 0.001. Comparisons without labels are not significant.

expression of the tight junction gene *Cldn8* in WT IECs (Fig. 6). Last, we identified that the combination of clock disruption and CRC produces a significant increase in intestinal permeability in vivo (Fig. 7). Together, our findings indicate that the circadian clock plays a role in regulating intestinal barrier integrity and microbiome composition, and these effects are further exacerbated in the context of CRC.

Tight junctions are an important component of barrier function as they mediate paracellular permeability and their disruption can result in leakage of endotoxins into the circulation (*111*, *112*). We identified rhythmicity in *Cldn8* and a decrease in *Tjp1* expression upon *Bmal1* loss. The core clock, as a whole, may play an important role in regulating tight junctions, as a previous study found *Per2*-dependent rhythmicity in the expression of the tight junction genes *Claudin1* and *Occludin* in mouse colon (*22*). We identified an increase in intestinal permeability in some $Bmal1^{-/-}$ mice, which was greatly exacerbated when combined with CRC. A previous study found that circadian disruption resulted in barrier dysfunction, down-regulation of microbial pathways promoting beneficial host responses, and up-regulation of microbial genes involved in endotoxin production (*48*). Therefore, circadian disruption may play an important role in breakdown

of barrier function during CRC development through regulation of tight junction proteins.

We identified a significant increase in *F. mortiferum* in the microbiomes of the tumor-bearing $Apc^{+/-}$ and $Apc^{+/-}$;$Bmal1^{-/-}$ mice. Our findings are consistent with an enrichment of *Fusobacterium* in human CRC that has been previously reported across multiple studies (*51*, *53*, *65*, *119*–*127*), and *Fusobacterium* has been suggested to play a driver role in CRC by modulating Wnt signaling through FadA (*128*). We also found that *M. elsdenii* was clock and cancer associated, as it was elevated in $Apc^{+/-}$;$Bmal1^{-/-}$ intestinal microbiomes. *M. elsdenii* is a lactate-utilizing bacterium that has been linked to gastric cancer, but its association with CRC is unclear (*96*, *129*). We propose that, in advanced CRC, tumors produce significant amounts of lactate that fuels lactate-consuming bacteria. We previously reported altered metabolites including lactate, as well as nucleotides, amino acids, and lipids in our $Apc^{+/-}$;$Bmal1^{-/-}$ organoids using stable isotope tracing and metabolomics (*89*). In this study, we identified dysregulation of similar bacterial metabolic pathways related to nucleic acid, fatty acid, and amino acid metabolism upon tumor development. Further work using metabolic tracing is required to investigate potential cross-talk between bacteria and tumor-derived metabolites.

Many studies have identified an increase of the *Bacteroides* genus in patients with CRC, particularly *B. fragilis* (*52*, *53*, *60*, *64*, *68*, *119*, *130*), although others have reported opposite data (*55*, *63*, *66*, *131*). This highlights a challenge with microbiome studies with inter-study differences that could be due to experimental methods, cancer heterogeneity, environmental conditions, or geography (*97*, *132*, *133*). We identified a clock-related increase in the abundance of many different *Bacteroides* species, which have a wide capacity to degrade complex carbohydrates (*134*, *135*). For example, *B. thetaiotaomicron* can switch its metabolism to host mucus-derived glycans when there are insufficient dietary polysaccharides (*136*), and over-colonization by mucus degrading bacteria can thin the mucus layer (*137*, *138*). In our model, we found a decreased expression of several mucin genes in $Bmal1^{-/-}$ IECs and $Apc^{+/-}$;$Bmal1^{-/-}$ tumors relative to WT IECs. We also identified reduced mucus staining in tumor regions of $Apc^{+/-}$ and $Apc^{+/-}$;$Bmal1^{-/-}$ mice, which is consistent with observations using the *Apc* mutant mouse model (*139*). However, in our microbial pathway analysis, we identified a reduction in the degradation of mucus sugars such as hexuronates and galactose by $Apc^{+/-}$;$Bmal1^{-/-}$ microbiomes. One possible explanation is that clock-mediated increase in *Bacteroides* species results in increased mucus degradation and thinning of the mucus membrane. Less mucus abundance would subsequently shift bacteria away from mucus-dependent polysaccharide metabolism toward other metabolic sources. An alternative possibility is that, during tumor development, a shift toward a stem-like state results in a reduction of differentiated cells such as secretory or goblet cells that control mucus secretion. In turn, less host mucus production would shift microbial metabolism away from mucus degradation. Further work is needed to better define these alterations in mucus metabolism in vivo.

A temporal rhythm in bacterial abundance has been previously reported that is genotype-dependent and heavily influenced by feeding (*24*, *28*, *43*, *46*). A previous study found that *Per1/2* deletion resulted in the loss of rhythmic fluctuations in commensal bacterial abundance including *Bacteroidales*, while light feeding shifted the rhythm of cycling operational taxonomic units (OTUs) including those of the *Bacteroides* genus (*42*). In addition, *Bmal1* loss resulted in nonrhythmic and more abundant *Bacteroides* (*44*). A recent study identified that loss of intestinal *Bmal1* results in more than half of rhythmic OTUs becoming arrhythmic (*45*). At the phylum level, both *Firmicutes* and *Bacteroidetes* rhythmicity was maintained in $Bmal1^{-/-}$ by relative abundance analysis, but there was loss of rhythmicity of Firmicutes by quantitative analysis upon intestine-specific *Bmal1* loss (*45*). Further longitudinal studies are needed to define whether alterations in rhythmicity of bacterial abundance affect CRC development, and this is especially relevant given the alarming increase in early-onset CRC cases where dietary and lifestyle factors likely contribute to the underlying disease etiology (*140*–*142*). Collectively, our data further implicates the circadian clock in maintaining intestinal homeostasis and delineates how disruption of the clock is involved in susceptibility to stressors such as CRC.

Limitations of the study

We have focused on the effects of clock disruption on the microbiome relative to intestinal tumor development. However, our study does not causally link these clock-modulated bacteria to enhanced CRC severity. Future studies are required, for example, monocolonization with key *Bacteroides* species, to determine whether these bacteria can drive CRC development and help to delineate how microbiota interventions can affect disease phenotype.

MATERIALS AND METHODS

Mice

Mice containing flox sites flanking one allele of *Apc* exons 1 to 15 ($Apc^{+/\Delta ex1\text{-}15}$) (the Jackson Laboratory, strain 009045) (*143*) were crossed with mice with flox sites flanking both alleles of exon 8 of *Bmal1* ($Bmal1^{fl/fl}$) (the Jackson Laboratory, strain 007668) (*144*). These mice were crossed with Villin-Cre mice (the Jackson Laboratory, strain 004586) (*145*) to create intestine-specific $Apc^{+/\Delta ex1\text{-}15}$;$Bmal1^{fl/fl}$ animals. Experiments were performed in compliance with the Institutional Animal Care and Use Committee (IACUC) guidelines at the University of California, Irvine (IACUC study number AUP-23-069). Mice were kept in standard 12-hour light/dark paradigm and fed ad libitum. Experiments were performed with 10-month-old mice, and groups contained even split of males and females.

Microbiome sequencing

Fecal samples were collected during the middle of the light period at ZT8 to minimize differences in food intake between mice. Sample size of 8 to 10 mice was chosen to allow for the variability usually seen in microbiome data (*97*, *132*, *133*). Feces were homogenized with 1 ml of DNA/RNA shield (Zymo Research, Irvine, CA). Fecal samples were processed, sequenced, and analyzed by Zymo Research (Irvine, CA) with the ZymoBIOMICS Shotgun Metagenomic Sequencing Service for Microbiome Analysis. In brief, DNA was extracted using the ZymoBIOMICS-96 MagBead DNA Kit (Zymo Research, Irvine, CA). Sequencing libraries were prepared with the Nextera DNA Flex Library Prep Kit (Illumina, San Diego, CA) using 100 ng of DNA input and internal dual-index 8–base pair (bp) barcodes with Nextera adapters (Illumina, San Diego, CA) according to the manufacturers protocol. All libraries were quantified with TapeStation (Agilent Technologies, Santa Clara, CA) and then pooled in equal abundance. The final pool was quantified using qPCR, and the library was sequenced on the Illumina NovaSeq (San Diego, CA). Raw sequence reads were trimmed with Trimmomatic-0.33 quality trimming with a 6-bp sliding window, a quality cutoff of 20, and a length cutoff of

70 bp (*146*). Microbial composition was profiled with Centrifuge (*147*) using bacterial, viral, fungal, mouse, and human genome datasets. Strain-level abundance information was extracted from the Centrifuge outputs and further analyzed. α-Diversity analysis was performed using the phyloseq package in R. Statistical significance was determined using the Wilcoxon signed-rank test. β-Diversity analysis was performed in R using the vegan and ecodist packages with Bray-Curtis distances followed by graphing using ggplot2 and the stat ellipse function. ANOSIM analysis was performed in R using the vegan and ggvegan packages using the Gower distance method. To perform functional analysis, mouse and viral DNA were first removed using KneadData followed by functional pathway analysis using HUMAnN with the ChocoPhlAn nucleotide and uniref90 protein databases (*98*). Significance of bacterial species abundance (Centrifuge) and functional pathway abundance (HUMAnN) was determined using MaAsLin2 with default parameters and a q value significance threshold of 0.25 (*94*). Biomarker discovery was performed using LEfSe (*95*) with default settings ($P > 0.05$ and LDA effect size > 2).

Intestinal organoid culture

The following protocol was used for intestinal crypt isolation and organoid isolation based on previously published methods (*89*, *148*). The ileum from mice of each genotype was dissected, washed with cold phosphate-buffered saline (PBS), and opened longitudinally. The intestine was cut into 2- to 5-mm pieces and rotated in cold PBS, with 2 mM EDTA and 10 μM Rho kinase (ROCK) inhibitor (Y-27632) for 1 hour. Next, tissue pieces were shaken vigorously in cold PBS and filtered with a 70-μm cell strainer. Crypt-enriched fractions were centrifuged at 290*g* and resuspended in 50 μl of growth factor reduced Matrigel (Corning Inc.). After Matrigel polymerization, epidermal growth factor (EGF)-Noggin-R-spondin (ENR) medium was added. ENR was prepared by adding 3 mM L-glutamine, primocin (50 mg/ml), 10 mM Hepes, recombinant murine EGF (50 ng/ml; PeproTech), recombinant murine Noggin (50 ng/ml; PeproTech), 1 mM *N*-acetylcysteine, and 20% v/v of R-spondin conditioned medium (Cultrex Rspo1-expressing cells, Trevigen) to Advanced Dulbecco's modified Eagle's medium/Ham's F12 medium. After 5 to 7 days, organoids were passaged by solubilizing Matrigel in ice-cold PBS for 10 min and centrifuging. Pelleted organoids were resuspended in basal medium (ENR medium without growth factors), vigorously broken apart by pipetting, and centrifuged. Organoid pellets were then resuspended in Matrigel and plated in 24-well plates. After polymerization at 37°C, ENR medium was added.

Western blot

Intestinal organoid pellets were lysed in ice-cold radioimmunoprecipitation assay lysis buffer [50 mM tris (pH 8), 150 mM NaCl, 5 mM EDTA, 15 mM $MgCl_2$, and 1% NP-40] containing appropriate inhibitors [1× complete EDTA-free cocktail tablet (Sigma-Aldrich), 0.5 mM phenylmethylsulfonyl fluoride, 20 mM NaF, 1 mM Na_3VO_4, and 1 μM trichostatin A]. Lysates were centrifugated, and protein concentration of supernatant was measured using Bradford reagent (Thermo Fisher Scientific). Protein lysates were resolved on an SDS–polyacrylamide gel electrophoresis gel and immunoblotting performed using BMAL1 (Abcam, ab93806) and α-tubulin (Sigma-Aldrich, T516B) antibodies.

IEC dissociation

Mice were housed in 12-hour light/12-hour dark conditions and sacrificed at the required ZT. Mouse ileum was dissected, cut longitudinally, and washed in PBS. The tissue was shaken vigorously in wash solution [Hanks' balanced salt solution with 15 mM Hepes (Sigma-Aldrich) and 1% penicillin/streptomycin] and centrifuged at 720*g* and 4°C. The intestine was shaken vigorously for 30 s and incubated at 37°C for 10 min in wash solution supplemented with 10 mM EDTA and 5% fetal bovine serum (FBS). After vigorously shaking again, tissue pieces were removed, and cells were collected by centrifugation at 720*g*, 4°C. The cells were washed with PBS once and pelleted for further analysis.

RNA isolation, cDNA synthesis, and qPCR

For intestinal organoids, RNA was isolated using the Direct-Zol RNA microprep kit (Zymo Research, R2060), according to the manufacturer's recommendation. Samples were prepared together to avoid introducing technical bias. For IECs and Caco-2 cells, RNA was isolated using Trizol reagent according to manufacturer's recommendations. To synthesize cDNA, 1 μg of RNA was incubated with the Maxima H Minus cDNA Synthesis Master Mix (Life Technologies, Thermo Fisher Scientific, M1662). Equivalent amounts of cDNA were combined with 0.3 μM forward and reverse primers and 1× PowerUp SYBR green Master Mix (Applied Biosystems, A25741). 18*S* ribosomal RNA primers were used to normalize gene expression. All primers used in qPCR experiments are listed in table S1. To determine statistical significance, Student's unpaired t test or one-way analysis of variance (ANOVA) with Tukey's multiple comparisons was used depending on the number of groups as recommended by GraphPad Prism version 10. Circadian period, phase, amplitude, goodness of fit, and rhythmicity P value were calculated for each replicate using BioDare2 linear detrending Fast Fourier Transform Non Linear Least Squares (FFT NLLS) and averaged (*149*).

Organoid RNA-seq

Full details of the experimental methods and analysis have been previously reported (*89*). In brief, crypts were isolated from each genotype, and intestinal organoids were derived and cultured using Matrigel and required growth factors. Unsynchronized organoids were collected for RNA isolation as previously described (*89*). Reads were aligned and quantified, and differential expression analysis (DESeq2) was performed as previously described (*89*). DESeq2 statistical approach was used as this enables quantitative analysis determining the strength of differential expression and adjusts for small replicate numbers and a large dynamic range (*150*).

Caco-2 culture and barrier function test

Caco-2 cell line (American Type Culture Collection, HTB-37) derived from human male colon was grown in Eagle's minimal essential medium (EMEM) culture medium (ECM) supplemented with 20% FBS, 1% penicillin/streptomycin, 1% nonessential amino acids, and sodium pyruvate (0.11 g/liter). Caco-2 monolayers were established using cells at passages 2 to 6 according to a previously published rapid method (*151*). Twenty-four–well 1.0 μM Transwell permeable inserts (Corning) were coated with collagen I (5 $\mu g/cm^2$). Cells were seeded at 0.5×10^5 to 1×10^5 cells per well and incubated in ECM with 0.1% MITO+ serum extender (Corning). After 24 hours, the medium was changed to ECM containing 0.1% MITO+ and 2 mM sodium butyrate. Monolayers were used 72 hours after seeding when confluency had been confirmed by light microscopy. Barrier tests were performed by adding 4-kDa FITC-dextran (1 mg/ml) to the apical compartment and collecting medium from the basal

compartment every 15 min. Fluorescence was measured at 485/515 nm alongside a FITC-dextran standard curve. Cumulative FITC-dextran was plotted against time to determine FITC-dextran transport in nanograms per milliliter per minute. Monolayers or confluent cells were synchronized with 1 mM dexamethasone for 1 hour.

FITC-dextran permeability assay

Mice were fasted for 12 to 16 hours before gavage. At ZT23, mice were gavaged with 4-kDa FITC-dextran (600 mg/kg; Sigma-Aldrich). After 1 hour, mice were euthanized, and blood was collected. To collect serum, blood was coagulated for 30 min at room temperature and spun at 800*g*. Fluorescence was measured in diluted serum at 530 nm with excitation at 485 nm, and 4-kDa FITC-dextran concentration was determined using a standard curve from 0 to 8000 ng/ml.

Histology

Flushed and linearized small intestines were fixed in Bouin's solution and then paraffin embedded and sectioned by the Chao Family Comprehensive Cancer Center Experimental Tissue Resource. Slides were rehydrated and incubated in 0.5% periodic acid for 5 min, Schiff's reagent for 15 min, and Harris modified hematoxylin for 90 s with washes in water in between. After dehydration, slides were mounted with VECTASHIELD (Vector Laboratories).

Supplementary Materials

This PDF file includes:

Figs. S1 to S6
Tables S1 and S2

REFERENCES AND NOTES

1. A. Verlande, S. Masri, Circadian clocks and cancer: Timekeeping governs cellular metabolism. *Trends Endocrinol. Metab.* **30**, 445–458 (2019).
2. J. Bass, M. A. Lazar, Circadian time signatures of fitness and disease. *Science* **354**, 994–999 (2016).
3. A. Chaix, A. Zarrinpar, S. Panda, The circadian coordination of cell biology. *J. Cell Biol.* **215**, 15–25 (2016).
4. K. H. Cox, J. S. Takahashi, Circadian clock genes and the transcriptional architecture of the clock mechanism. *J. Mol. Endocrinol.* **63**, R93–R102 (2019).
5. B. J. Altman, A. L. Hsieh, A. Sengupta, S. Y. Krishnanaiah, Z. E. Stine, Z. E. Walton, A. M. Gouw, A. Venkataraman, B. Li, P. Goraksha-Hicks, S. J. Diskin, D. I. Bellovin, M. C. Simon, J. C. Rathmell, M. A. Lazar, J. M. Maris, D. W. Felsher, J. B. Hogenesch, A. M. Weljie, C. V. Dang, MYC disrupts the circadian clock and metabolism in cancer cells. *Cell Metab.* **22**, 1009–1019 (2015).
6. R. A. Akhtar, A. B. Reddy, E. S. Maywood, J. D. Clayton, V. M. King, A. G. Smith, T. W. Gant, M. H. Hastings, C. P. Kyriacou, Circadian cycling of the mouse liver transcriptome, as revealed by cDNA microarray, is driven by the suprachiasmatic. *Curr. Biol.* **12**, 540–550 (2002).
7. S. Panda, M. P. Antoch, B. H. Miller, A. I. Su, A. B. Schook, M. Straume, P. G. Schultz, S. A. Kay, J. S. Takahashi, J. B. Hogenesch, Coordinated transcription of key pathways in the mouse by the circadian clock. *Cell* **109**, 307–320 (2002).
8. S. Masri, P. Sassone-Corsi, The circadian clock: A framework linking metabolism, epigenetics and neuronal function. *Nat. Rev. Neurosci.* **14**, 69–75 (2013).
9. C. L. Partch, C. B. Green, J. S. Takahashi, Molecular architecture of the mammalian circadian clock. *Trends Cell Biol.* **24**, 90–99 (2014).
10. T. Matsu-ura, A. Dovzhenok, E. Aihara, J. Rood, H. Le, Y. Ren, A. E. Rosselot, T. Zhang, C. Lee, K. Obrietan, M. H. Montrose, S. Lim, S. R. Moore, C. I. Hong, Intercellular coupling of the cell cycle and circadian clock in adult stem cell culture. *Mol. Cell* **64**, 900–912 (2016).
11. K. Parasram, N. Bernardon, M. Hammoud, H. Chang, L. He, N. Perrimon, P. Karpowicz, Intestinal stem cells exhibit conditional circadian clock function. *Stem Cell Rep.* **11**, 1287–1301 (2018).
12. M. Soták, L. Polidarová, P. Ergang, A. Sumová, J. Pácha, An association between clock genes and clock-controlled cell cycle genes in murine colorectal tumors. *Int. J. Cancer* **132**, 1032–1041 (2013).
13. C. I. Hong, J. Zámborszky, M. Baek, L. Labiscsak, K. Ju, H. Lee, L. F. Larrondo, A. Goity, H. S. Chong, W. J. Belden, A. Csikász-Nagy, Circadian rhythms synchronize mitosis in *Neurospora crassa*. *Proc. Natl. Acad. Sci. U.S.A.* **111**, 1397–1402 (2014).
14. Q. Yang, B. F. Pando, G. Dong, S. S. Golden, A. van Oudenaarden, Circadian gating of the cell cycle revealed in single cyanobacterial cells. *Science* **327**, 1522–1526 (2010).
15. P. Karpowicz, Y. Zhang, J. B. Hogenesch, P. Emery, N. Perrimon, The circadian clock gates the intestinal stem cell regenerative state. *Cell Rep.* **3**, 996–1004 (2013).
16. A. C. Silver, A. Arjona, M. E. Hughes, M. N. Nitabach, E. Fikrig, Circadian expression of clock genes in mouse macrophages, dendritic cells, and B cells. *Brain Behav. Immun.* **26**, 407–413 (2012).
17. M. Keller, J. Mazuch, U. Abraham, G. D. Eom, E. D. Herzog, H.-D. Volk, A. Kramer, B. Maier, A circadian clock in macrophages controls inflammatory immune responses. *Proc. Natl. Acad. Sci. U.S.A.* **106**, 21407–21412 (2009).
18. J. E. Gibbs, J. Blaikley, S. Beesley, L. Matthews, K. D. Simpson, S. H. Boyce, S. N. Farrow, K. J. Else, D. Singh, D. W. Ray, A. S. I. Loudon, The nuclear receptor REV-ERBα mediates circadian regulation of innate immunity through selective regulation of inflammatory cytokines. *Proc. Natl. Acad. Sci. U.S.A.* **109**, 582–587 (2012).
19. S. Kiessling, G. Dubeau-Laramée, H. Ohm, N. Labrecque, M. Olivier, N. Cermakian, The circadian clock in immune cells controls the magnitude of Leishmania parasite infection. *Sci. Rep.* **7**, 10892 (2017).
20. K. C. Summa, R. M. Voigt, C. B. Forsyth, M. Shaikh, K. Cavanaugh, Y. Tang, M. H. Vitaterna, S. Song, F. W. Turek, A. Keshavarzian, Disruption of the circadian clock in mice increases intestinal permeability and promotes alcohol-induced hepatic pathology and inflammation. *PLOS ONE* **8**, e67102 (2013).
21. L. Tran, S. B. Jochum, M. Shaikh, S. Wilber, L. Zhang, D. M. Hayden, C. B. Forsyth, R. M. Voigt, F. Bishehsari, A. Keshavarzian, G. R. Swanson, Circadian misalignment by environmental light/dark shifting causes circadian disruption in colon. *PLOS ONE* **16**, e0251604 (2021).
22. O. Kyoko, H. Kono, K. Ishimaru, K. Miyake, T. Kubota, H. Ogawa, K. Okumura, S. Shibata, A. Nakao, Expressions of tight junction proteins occludin and claudin-1 are under the circadian control in the mouse large intestine: Implications in intestinal permeability and susceptibility to colitis. *PLOS ONE* **9**, e98016 (2014).
23. R. M. Voigt, C. B. Forsyth, M. Shaikh, L. Zhang, S. Raeisi, C. Aloman, N. Z. Preite, T. M. Donohue Jr., L. Fogg, A. Keshavarzian, Diurnal variations in intestinal barrier integrity and liver pathology in mice: Implications for alcohol binge. *Am. J. Physiol. Gastrointest. Liver Physiol.* **314**, G131–G141 (2018).
24. A. Zarrinpar, A. Chaix, S. Yooseph, S. Panda, Diet and feeding pattern affect the diurnal dynamics of the gut microbiome. *Cell Metab.* **20**, 1006–1017 (2014).
25. T. Tuganbaev, U. Mor, S. Bashiardes, T. Liwinski, S. P. Nobs, A. Leshem, M. Dori-Bachash, C. A. Thaiss, E. Y. Pinker, K. Ratiner, L. Adlung, S. Federici, C. Kleimeyer, C. Moresi, T. Yamada, Y. Cohen, X. Zhang, H. Massalha, E. Massasa, Y. Kuperman, P. A. Koni, A. Harmelin, N. Gao, S. Itzkovitz, K. Honda, H. Shapiro, E. Elinav, Diet diurnally regulates small intestinal microbiome-epithelial-immune homeostasis and enteritis. *Cell* **182**, 1441–1459.e21 (2020).
26. K. P. Kelly, K. L. J. Ellacott, H. Chen, O. P. McGuinness, C. H. Johnson, Time-optimized feeding is beneficial without enforced fasting. *Open Biol.* **11**, 210183 (2021).
27. S. Deota, T. Lin, A. Chaix, A. Williams, H. Le, H. Calligaro, R. Ramasamy, L. Huang, S. Panda, Diurnal transcriptome landscape of a multi-tissue response to time-restricted feeding in mammals. *Cell Metab.* **35**, 150–165.e4 (2023).
28. V. Leone, S. M. Gibbons, K. Martinez, A. L. Hutchison, E. Y. Huang, C. M. Cham, J. F. Pierre, A. F. Heneghan, A. Nadimpalli, N. Hubert, E. Zale, Y. Wang, Y. Huang, B. Theriault, A. R. Dinner, M. W. Musch, K. A. Kudsk, B. J. Prendergast, J. A. Gilbert, E. B. Chang, Effects of diurnal variation of gut microbes and high-fat feeding on host circadian clock function and metabolism. *Cell Host Microbe.* **17**, 681–689 (2015).
29. M. Ulgherait, A. M. Midoun, S. J. Park, J. A. Gatto, S. J. Tener, J. Siewert, N. Klickstein, J. C. Canman, W. W. Ja, M. Shirasu-Hiza, Circadian autophagy drives iTRF-mediated longevity. *Nature* **598**, 353–358 (2021).
30. E. G. Zoetendal, J. Raes, B. van den Bogert, M. Arumugam, C. C. G. M. Booijink, F. J. Troost, P. Bork, M. Wels, W. M. de Vos, M. Kleerebezem, The human small intestinal microbiota is driven by rapid uptake and conversion of simple carbohydrates. *ISME J.* **6**, 1415–1426 (2012).
31. A. W. Walker, J. Ince, S. H. Duncan, L. M. Webster, G. Holtrop, X. Ze, D. Brown, M. D. Stares, P. Scott, A. Bergerat, P. Louis, F. McIntosh, A. M. Johnstone, G. E. Lobley, J. Parkhill, H. J. Flint, Dominant and diet-responsive groups of bacteria within the human colonic microbiota. *ISME J.* **5**, 220–230 (2011).
32. H. Daniel, A. M. Gholami, D. Berry, C. Desmarchelier, H. Hahne, G. Loh, S. Mondot, P. Lepage, M. Rothballer, A. Walker, C. Böhm, M. Wenning, M. Wagner, M. Blaut, P. Schmitt-Kopplin, B. Kuster, D. Haller, T. Clavel, High-fat diet alters gut microbiota physiology in mice. *ISME J.* **8**, 295–308 (2014).
33. A. Visconti, C. I. Le Roy, F. Rosa, N. Rossi, T. C. Martin, R. P. Mohney, W. Li, E. de Rinaldis, J. T. Bell, J. C. Venter, K. E. Nelson, T. D. Spector, M. Falchi, Interplay between the human gut microbiome and host metabolism. *Nat. Commun.* **10**, 4505 (2019).

34. A. J. Macpherson, M. B. Geuking, K. D. McCoy, Immune responses that adapt the intestinal mucosa to commensal intestinal bacteria. *Immunology* **115**, 153–162 (2005).
35. H. Chu, S. K. Mazmanian, Innate immune recognition of the microbiota promotes host-microbial symbiosis. *Nat. Immunol.* **14**, 668–675 (2013).
36. D. Zheng, T. Liwinski, E. Elinav, Interaction between microbiota and immunity in health and disease. *Cell Res.* **30**, 492–506 (2020).
37. A. M. Kabat, N. Srinivasan, K. J. Maloy, Modulation of immune development and function by intestinal microbiota. *Trends Immunol.* **35**, 507–517 (2014).
38. B. D. Needham, M. Funabashi, M. D. Adame, Z. Wang, J. C. Boktor, J. Haney, W.-L. Wu, C. Rabut, M. S. Ladinsky, S.-J. Hwang, Y. Guo, Q. Zhu, J. A. Griffiths, R. Knight, P. J. Bjorkman, M. G. Shapiro, D. H. Geschwind, D. P. Holschneider, M. A. Fischbach, S. K. Mazmanian, A gut-derived metabolite alters brain activity and anxiety behaviour in mice. *Nature* **602**, 647–653 (2022).
39. G. Sharon, N. J. Cruz, D.-W. Kang, M. J. Gandal, B. Wang, Y.-M. Kim, E. M. Zink, C. P. Casey, B. C. Taylor, C. J. Lane, L. M. Bramer, N. G. Isern, D. W. Hoyt, C. Noecker, M. J. Sweredoski, A. Moradian, E. Borenstein, J. K. Jansson, R. Knight, T. O. Metz, C. Lois, D. H. Geschwind, R. Krajmalnik-Brown, S. K. Mazmanian, Human gut microbiota from autism spectrum disorder promote behavioral symptoms in mice. *Cell* **177**, 1600–1618.e17 (2019).
40. C. A. Olson, H. E. Vuong, J. M. Yano, Q. Y. Liang, D. J. Nusbaum, E. Y. Hsiao, The gut microbiota mediates the anti-seizure effects of the ketogenic diet. *Cell* **173**, 1728–1741.e13 (2018).
41. H. E. Vuong, G. N. Pronovost, D. W. Williams, E. J. L. Coley, E. L. Siegler, A. Qiu, M. Kazantsev, C. J. Wilson, T. Rendon, E. Y. Hsiao, The maternal microbiome modulates fetal neurodevelopment in mice. *Nature* **586**, 281–286 (2020).
42. C. A. Thaiss, M. Levy, T. Korem, L. Dohnalová, H. Shapiro, D. A. Jaitin, E. David, D. R. Winter, M. Gury-BenAri, E. Tatirovsky, T. Tuganbaev, S. Federici, N. Zmora, D. Zeevi, M. Dori-Bachash, M. Pevsner-Fischer, E. Kartvelishvily, A. Brandis, A. Harmelin, O. Shibolet, Z. Halpern, K. Honda, I. Amit, E. Segal, E. Elinav, Microbiota diurnal rhythmicity programs host transcriptome oscillations. *Cell* **167**, 1495–1510.e12 (2016).
43. R. M. Voigt, C. B. Forsyth, S. J. Green, P. A. Engen, A. Keshavarzian, Circadian rhythm and the gut microbiome. *Int. Rev. Neurobiol.* **131**, 193–205 (2016).
44. X. Liang, F. D. Bushman, G. A. FitzGerald, Rhythmicity of the intestinal microbiota is regulated by gender and the host circadian clock. *Proc. Natl. Acad. Sci. U.S.A.* **112**, 10479–10484 (2015).
45. M. Heddes, B. Altaha, Y. Niu, S. Reitmeier, K. Kleigrewe, D. Haller, S. Kiessling, The intestinal clock drives the microbiome to maintain gastrointestinal homeostasis. *Nat. Commun.* **13**, 6068 (2022).
46. C. A. Thaiss, D. Zeevi, M. Levy, G. Zilberman-Schapira, J. Suez, A. C. Tengeler, L. Abramson, M. N. Katz, T. Korem, N. Zmora, Y. Kuperman, I. Biton, S. Gilad, A. Harmelin, H. Shapiro, Z. Halpern, E. Segal, E. Elinav, Transkingdom control of microbiota diurnal oscillations promotes metabolic homeostasis. *Cell* **159**, 514–529 (2014).
47. R. M. Voigt, C. B. Forsyth, S. J. Green, E. Mutlu, P. Engen, M. H. Vitaterna, F. W. Turek, A. Keshavarzian, Circadian disorganization alters intestinal microbiota. *PLOS ONE* **9**, e97500 (2014).
48. J. A. Deaver, S. Y. Eum, M. Toborek, Circadian disruption changes gut microbiome taxa and functional gene composition. *Front. Microbiol.* **9**, 737 (2018).
49. S. T. Anderson, H. Meng, T. G. Brooks, S. Y. Tang, R. Lordan, A. Sengupta, S. Nayak, A. Mřela, D. Sarantopoulou, N. F. Lahens, A. Weljie, G. R. Grant, F. D. Bushman, G. A. FitzGerald, Sexual dimorphism in the response to chronic circadian misalignment on a high-fat diet. *Sci. Transl. Med.* **15**, eabo2022 (2023).
50. I. Sobhani, J. Tap, F. Roudot-Thoraval, J. P. Roperch, S. Letulle, P. Langella, C. Gérard, J. T. van Nhieu, J. P. Furet, Microbial dysbiosis in colorectal cancer (CRC) patients. *PLOS ONE* **6**, e16393 (2011).
51. N. Wu, X. Yang, R. Zhang, J. Li, X. Xiao, Y. Hu, Y. Chen, F. Yang, N. Lu, Z. Wang, C. Luan, Y. Liu, B. Wang, C. Xiang, Y. Wang, F. Zhao, G. F. Gao, S. Wang, L. Li, H. Zhang, B. Zhu, Dysbiosis signature of fecal microbiota in colorectal cancer patients. *Microb. Ecol.* **66**, 462–470 (2013).
52. Q. Feng, S. Liang, H. Jia, A. Stadlmayr, L. Tang, Z. Lan, D. Zhang, H. Xia, X. Xu, Z. Jie, L. Su, X. Li, X. Li, J. Li, L. Xiao, U. Huber-Schönauer, D. Niederseer, X. Xu, J. Y. Al-Aama, H. Yang, J. Wang, K. Kristiansen, M. Arumugam, H. Tilg, C. Datz, J. Wang, Gut microbiome development along the colorectal adenoma-carcinoma sequence. *Nat. Commun.* **6**, 6528 (2015).
53. G. Nakatsu, X. Li, H. Zhou, J. Sheng, S. H. Wong, W. K. K. Wu, S. C. Ng, H. Tsoi, Y. Dong, N. Zhang, Y. He, Q. Kang, L. Cao, K. Wang, J. Zhang, Q. Liang, J. Yu, J. J. Y. Sung, Gut mucosal microbiome across stages of colorectal carcinogenesis. *Nat. Commun.* **6**, 8727 (2015).
54. J. Yu, Q. Feng, S. H. Wong, D. Zhang, Q. Y. Liang, Y. Qin, L. Tang, H. Zhao, J. Stenvang, Y. Li, X. Wang, X. Xu, N. Chen, W. K. K. Wu, J. Al-Aama, H. J. Nielsen, P. Kiilerich, B. A. H. Jensen, T. O. Yau, Z. Lan, H. Jia, J. Li, L. Xiao, T. Y. T. Lam, S. C. Ng, A. S.-L. Cheng, V. W.-S. Wong, F. K. L. Chan, X. Xu, H. Yang, L. Madsen, C. Datz, H. Tilg, J. Wang, N. Brünner, K. Kristiansen, M. Arumugam, J. J.-Y. Sung, J. Wang, Metagenomic analysis of faecal microbiome as a tool towards targeted non-invasive biomarkers for colorectal cancer. *Gut* **66**, 70–78 (2017).
55. C. Bundgaard-Nielsen, U. T. Baandrup, L. P. Nielsen, S. Sørensen, The presence of bacteria varies between colorectal adenocarcinomas, precursor lesions and non-malignant tissue. *BMC Cancer* **19**, 399 (2019).
56. Z. Dai, J. Zhang, Q. Wu, J. Chen, J. Liu, L. Wang, C. Chen, J. Xu, H. Zhang, C. Shi, Z. Li, H. Fang, C. Lin, D. Tang, D. Wang, The role of microbiota in the development of colorectal cancer. *Int. J. Cancer* **145**, 2032–2041 (2019).
57. E. Elinav, W. S. Garrett, G. Trinchieri, J. Wargo, The cancer microbiome. *Nat. Rev. Cancer* **19**, 371–376 (2019).
58. S. M. A. Kendong, R. A. R. Ali, K. N. M. Nawawi, H. F. Ahmad, N. M. Mokhtar, Gut dysbiosis and intestinal barrier dysfunction: Potential explanation for early-onset colorectal cancer. *Front. Cell. Infect. Microbiol.* **11**, 744606 (2021).
59. O. O. Coker, C. Liu, W. K. K. Wu, S. H. Wong, W. Jia, J. J. Y. Sung, J. Yu, Altered gut metabolites and microbiota interactions are implicated in colorectal carcinogenesis and can be non-invasive diagnostic biomarkers. *Microbiome* **10**, 35 (2022).
60. G. Zeller, J. Tap, A. Y. Voigt, S. Sunagawa, J. R. Kultima, P. I. Costea, A. Amiot, J. Böhm, F. Brunetti, N. Habermann, R. Hercog, M. Koch, A. Luciani, D. R. Mende, M. A. Schneider, P. Schrotz-King, C. Tournigand, J. T. Van Nhieu, T. Yamada, J. Zimmermann, V. Benes, M. Kloor, C. M. Ulrich, M. von Knebel Doeberitz, I. Sobhani, P. Bork, Potential of fecal microbiota for early-stage detection of colorectal cancer. *Mol. Syst. Biol.* **10**, 766 (2014).
61. M. Kim, E. Vogtmann, D. A. Ahlquist, M. E. Devens, J. B. Kisiel, W. R. Taylor, B. A. White, V. L. Hale, J. Sung, N. Chia, R. Sinha, J. Chen, Fecal metabolomic signatures in colorectal adenoma patients are associated with gut microbiota and early events of colorectal cancer pathogenesis. *mBio* **11**, e03186-19 (2020).
62. T.-W. Yang, W.-H. Lee, S.-J. Tu, W.-C. Huang, H.-M. Chen, T.-H. Sun, M.-C. Tsai, C.-C. Wang, H.-Y. Chen, C.-C. Huang, B.-H. Shiu, T.-L. Yang, H.-T. Huang, Y.-P. Chou, C.-H. Chou, Y.-R. Huang, Y.-R. Sun, C. Liang, F.-M. Lin, S.-Y. Ho, W.-L. Chen, S.-F. Yang, K.-C. Ueng, H.-D. Huang, C.-N. Huang, Y.-J. Jong, C.-C. Lin, Enterotype-based analysis of gut microbiota along the conventional adenoma-carcinoma colorectal cancer pathway. *Sci. Rep.* **9**, 10923 (2019).
63. J. P. Zackular, M. A. M. Rogers, M. T. Ruffin IV, P. D. Schloss, The human gut microbiome as a screening tool for colorectal cancer. *Cancer Prev. Res.* **7**, 1112–1121 (2014).
64. J. R. Marchesi, B. E. Dutilh, N. Hall, W. H. M. Peters, R. Roelofs, A. Boleij, H. Tjalsma, Towards the human colorectal cancer microbiome. *PLOS ONE* **6**, e20447 (2011).
65. M. Castellarin, R. L. Warren, J. D. Freeman, L. Dreolini, M. Krzywinski, J. Strauss, R. Barnes, P. Watson, E. Allen-Vercoe, R. A. Moore, R. A. Holt, *Fusobacterium nucleatum* infection is prevalent in human colorectal carcinoma. *Genome Res.* **22**, 299–306 (2012).
66. A. D. Kostic, D. Gevers, C. S. Pedamallu, M. Michaud, F. Duke, A. M. Earl, A. I. Ojesina, J. Jung, A. J. Bass, J. Tabernero, J. Baselga, C. Liu, R. A. Shivdasani, S. Ogino, B. W. Birren, C. Huttenhower, W. S. Garrett, M. Meyerson, Genomic analysis identifies association of *Fusobacterium* with colorectal carcinoma. *Genome Res.* **22**, 292–298 (2012).
67. I. Borozan, S. H. Zaidi, T. A. Harrison, A. I. Phipps, J. Zheng, S. Lee, Q. M. Trinh, R. S. Steinfelder, J. Adams, B. L. Banbury, S. I. Berndt, S. Brezina, D. D. Buchanan, S. Bullman, Y. Cao, A. B. Farris, J. C. Figueiredo, M. Giannakis, L. E. Heisler, J. L. Hopper, Y. Lin, X. Luo, R. Nishihara, E. R. Mardis, N. Papadopoulos, C. Qu, E. E. G. Reid, S. N. Thibodeau, S. Harlid, C. Y. Um, L. Hsu, A. Gsur, P. T. Campbell, S. Gallinger, P. A. Newcomb, S. Ogino, W. Sun, T. J. Hudson, V. Ferretti, U. Peters, Molecular and pathology features of colorectal tumors and patient outcomes are associated with *Fusobacterium nucleatum* and its subspecies *animalis*. *Cancer Epidemiol. Biomarkers Prev.* **31**, 210–220 (2021).
68. T. Wang, G. Cai, Y. Qiu, N. Fei, M. Zhang, X. Pang, W. Jia, S. Cai, L. Zhao, Structural segregation of gut microbiota between colorectal cancer patients and healthy volunteers. *ISME J.* **6**, 320–329 (2012).
69. A. D. Kostic, E. Chun, L. Robertson, J. N. Glickman, C. A. Gallini, M. Michaud, T. E. Clancy, D. C. Chung, P. Lochhead, G. L. Hold, E. M. El-Omar, D. Brenner, C. S. Fuchs, M. Meyerson, W. S. Garrett, *Fusobacterium nucleatum* potentiates intestinal tumorigenesis and modulates the tumor-immune microenvironment. *Cell Host Microbe* **14**, 207–215 (2013).
70. M. R. Rubinstein, X. Wang, W. Liu, Y. Hao, G. Cai, Y. W. Han, *Fusobacterium nucleatum* promotes colorectal carcinogenesis by modulating e-cadherin/β-catenin signaling via its FadA adhesin. *Cell Host Microbe* **14**, 195–206 (2013).
71. M. R. Rubinstein, J. E. Baik, S. M. Lagana, R. P. Han, W. J. Raab, D. Sahoo, P. Dalerba, T. C. Wang, Y. W. Han, *Fusobacterium nucleatum* promotes colorectal cancer by inducing Wnt/β-catenin modulator Annexin A1. *EMBO Rep.* **20**, e47638 (2019).
72. J. Roelands, P. J. K. Kuppen, E. I. Ahmed, R. Mall, T. Masoodi, P. Singh, G. Monaco, C. Raynaud, N. F. C. C. de Miranda, L. Ferraro, T. C. Carneiro-Lobo, N. Syed, A. Rawat, A. Awad, J. Decock, W. Mifsud, L. D. Miller, S. Sherif, M. G. Mohamed, D. Rinchai, M. Van den Eynde, R. W. Sayaman, E. Ziv, F. Bertucci, M. A. Petkar, S. Lorenz, L. S. Mathew, K. Wang, S. Murugesan, D. Chaussabel, A. L. Vahrmeijer, E. Wang, A. Ceccarelli, K. A. Fakhro, G. Zoppoli, A. Ballestrero, R. A. E. M. Tollenaar, F. M. Marincola, J. Galon, S. A. Khodor, M. Ceccarelli, W. Hendrickx, D. Bedognetti, An integrated tumor, immune and microbiome atlas of colon cancer. *Nat. Med.* **29**, 1273–1286 (2023).
73. R. J. Obiso Jr., A. O. Azghani, T. D. Wilkins, The Bacteroides fragilis toxin fragilysin disrupts the paracellular barrier of epithelial cells. *Infect. Immun.* **65**, 1431–1439 (1997).

74. S. Wu, K. C. Lim, J. Huang, R. F. Saidi, C. L. Sears, *Bacteroides fragilis* enterotoxin cleaves the zonula adherens protein, E-cadherin. *Proc. Natl. Acad. Sci. U.S.A.* **95**, 14979–14984 (1998).
75. S. Wu, P. J. Morin, D. Maouyo, C. L. Sears, *Bacteroides fragilis* enterotoxin induces c-Myc expression and cellular proliferation. *Gastroenterology* **124**, 392–400 (2003).
76. E. S. Schernhammer, F. Laden, F. E. Speizer, W. C. Willett, D. J. Hunter, I. Kawachi, C. S. Fuchs, G. A. Colditz, Night-shift work and risk of colorectal cancer in the Nurses' Health Study. *J. Natl. Cancer Inst.* **95**, 825–828 (2003).
77. E. S. Schernhammer, C. H. Kroenke, F. Laden, S. E. Hankinson, Night work and risk of breast cancer. *Epidemiology* **17**, 108–111 (2006).
78. E. S. Schernhammer, P. Razavi, T. Y. Li, A. A. Qureshi, J. Han, Rotating night shifts and risk of skin cancer in the nurses' health study. *J. Natl. Cancer Inst.* **103**, 602–606 (2011).
79. E. S. Schernhammer, D. Feskanich, G. Liang, J. Han, Rotating night-shift work and lung cancer risk among female nurses in the United States. *Am. J. Epidemiol.* **178**, 1434–1441 (2013).
80. J. Hansen, C. F. Lassen, Nested case-control study of night shift work and breast cancer risk among women in the Danish military. *Occup. Environ. Med.* **69**, 551–556 (2012).
81. M.-É. Parent, M. El-Zein, M.-C. Rousseau, J. Pintos, J. Siemiatycki, Night work and the risk of cancer among men. *Am. J. Epidemiol.* **176**, 751–759 (2012).
82. B. D. Carter, W. R. Diver, J. S. Hildebrand, A. V. Patel, S. M. Gapstur, Circadian disruption and fatal ovarian cancer. *Am. J. Prev. Med.* **46**, S34–S41 (2014).
83. K. Papantoniou, G. Castaño-Vinyals, A. Espinosa, M. C. Turner, M. H. Alonso-Aguado, V. Martin, N. Aragonés, B. Pérez-Gómez, B. M. Pozo, I. Gómez-Acebo, E. Ardanaz, J. M. Altzibar, R. Peiro, A. Tardon, J. A. Lorca, M. D. Chirlaque, A. García-Palomo, J. J. Jimenez-Moleon, T. Dierssen, M. Ederra, P. Amiano, M. Pollan, V. Moreno, M. Kogevinas, Shift work and colorectal cancer risk in the MCC-Spain case-control study. *Scand. J. Work Environ. Health* **43**, 250–259 (2017).
84. E. Cordina-Duverger, F. Menegaux, A. Popa, S. Rabstein, V. Harth, B. Pesch, T. Brüning, L. Fritschi, D. C. Glass, J. S. Heyworth, T. C. Erren, G. Castaño-Vinyals, K. Papantoniou, A. Espinosa, M. Kogevinas, A. Grundy, J. J. Spinelli, K. J. Aronson, P. Guénel, Night shift work and breast cancer: A pooled analysis of population-based case-control studies with complete work history. *Eur. J. Epidemiol.* **33**, 369–379 (2018).
85. M. E. Jones, M. J. Schoemaker, E. C. McFadden, L. B. Wright, L. E. Johns, A. J. Swerdlow, Night shift work and risk of breast cancer in women: The generations study cohort. *Br. J. Cancer* **121**, 172–179 (2019).
86. International Agency for Research on Cancer, *Night Shift Work IARC Monographs on the Identification of Carcinogenic Hazards to Humans* (World Health Organization, ed. 1, 2020), vol. 124; https://publications.iarc.fr/Book-And-Report-Series/Iarc-Monographs-On-The-Identification-Of-Carcinogenic-Hazards-To-Humans/Night-Shift-Work-2020.
87. P. A. Wood, X. Yang, A. Taber, E.-Y. Oh, C. Ansell, S. E. Ayers, Z. Al-Assaad, K. Carnevale, F. G. Berger, M. M. O. Peña, W. J. M. Hrushesky, Period 2 mutation accelerates $Apc^{Min/+}$ tumorigenesis. *Mol. Cancer Res.* **6**, 1786–1793 (2008).
88. K. Stokes, M. Nunes, C. Trombley, D. E. F. L. Flôres, G. Wu, Z. Taleb, A. Alkhateeb, S. Banskota, C. Harris, O. P. Love, W. I. Khan, L. Rueda, J. B. Hogenesch, P. Karpowicz, The circadian clock gene, *Bmal1*, regulates intestinal stem cell signaling and represses tumor initiation. *Cell. Mol. Gastroenterol. Hepatol.* **12**, 1847–1872.e0 (2021).
89. S. K. Chun, B. M. Fortin, R. C. Fellows, A. N. Habowski, A. Verlande, W. A. Song, A. L. Mahieu, A. E. Y. T. Lefebvre, J. N. Sterrenberg, L. M. Velez, M. A. Digman, R. A. Edwards, N. R. Pannunzio, M. M. Seldin, M. L. Waterman, S. Masri, Disruption of the circadian clock drives *Apc* loss of heterozygosity to accelerate colorectal cancer. *Sci. Adv.* **8**, eabo2389 (2022).
90. X. Fan, Y. Jin, G. Chen, X. Ma, L. Zhang, Gut microbiota Dysbiosis drives the development of colorectal cancer. *Digestion* **102**, 508–515 (2021).
91. M. Schmitt, F. R. Greten, The inflammatory pathogenesis of colorectal cancer. *Nat. Rev. Immunol.* **21**, 653–667 (2021).
92. J. C. Arthur, E. Perez-Chanona, M. Mühlbauer, S. Tomkovich, J. M. Uronis, T.-J. Fan, B. J. Campbell, T. Abujamel, B. Dogan, A. B. Rogers, J. M. Rhodes, A. Stintzi, K. W. Simpson, J. J. Hansen, T. O. Keku, A. A. Fodor, C. Jobin, Intestinal inflammation targets cancer-inducing activity of the microbiota. *Science* **338**, 120–123 (2012).
93. V. Sethi, S. Kurtom, M. Tarique, S. Lavania, Z. Malchiodi, L. Hellmund, L. Zhang, U. Sharma, B. Giri, B. Garg, A. Ferrantella, S. M. Vickers, S. Banerjee, R. Dawra, S. Roy, S. Ramakrishnan, A. Saluja, V. Dudeja, Gut microbiota promotes tumor growth in mice by modulating immune response. *Gastroenterology* **155**, 33–37.e6 (2018).
94. H. Mallick, A. Rahnavard, L. J. McIver, S. Ma, Y. Zhang, L. H. Nguyen, T. L. Tickle, G. Weingart, B. Ren, E. H. Schwager, S. Chatterjee, K. N. Thompson, J. E. Wilkinson, A. Subramanian, Y. Lu, L. Waldron, J. N. Paulson, E. A. Franzosa, H. C. Bravo, C. Huttenhower, Multivariable association discovery in population-scale meta-omics studies. *PLoS Comput. Biol.* **17**, e1009442 (2021).
95. N. Segata, J. Izard, L. Waldron, D. Gevers, L. Miropolsky, W. S. Garrett, C. Huttenhower, Metagenomic biomarker discovery and explanation. *Genome Biol.* **12**, R60 (2011).
96. L. Chen, Y. Shen, C. Wang, L. Ding, F. Zhao, M. Wang, J. Fu, H. Wang, *Megasphaera elsdenii* lactate degradation pattern shifts in rumen acidosis models. *Front. Microbiol.* **10**, 162 (2019).
97. H. J. Flint, K. P. Scott, P. Louis, S. H. Duncan, The role of the gut microbiota in nutrition and health. *Nat. Rev. Gastroenterol. Hepatol.* **9**, 577–589 (2012).
98. F. Beghini, L. J. McIver, A. Blanco-Míguez, L. Dubois, F. Asnicar, S. Maharjan, A. Mailyan, P. Manghi, M. Scholz, A. M. Thomas, M. Valles-Colomer, G. Weingart, Y. Zhang, M. Zolfo, C. Huttenhower, E. A. Franzosa, N. Segata, Integrating taxonomic, functional, and strain-level profiling of diverse microbial communities with bioBakery 3. *eLife* **10**, e65088 (2021).
99. M. M. Adeva-Andany, M. González-Lucán, C. Donapetry-García, C. Fernández-Fernández, E. Ameneiros-Rodríguez, Glycogen metabolism in humans. *BBA Clin.* **5**, 85–100 (2016).
100. M. C. Rose, J. A. Voynow, Respiratory tract mucin genes and mucin glycoproteins in health and disease. *Physiol. Rev.* **86**, 245–278 (2006).
101. P. Paone, P. D. Cani, Mucus barrier, mucins and gut microbiota: The expected slimy partners? *Gut* **69**, 2232–2243 (2020).
102. J. Fang, H. Wang, Y. Zhou, H. Zhang, H. Zhou, X. Zhang, Slimy partners: The mucus barrier and gut microbiome in ulcerative colitis. *Exp. Mol. Med.* **53**, 772–787 (2021).
103. S. Jäger, E. F. Stange, J. Wehkamp, Inflammatory bowel disease: An impaired barrier disease. *Langenbecks Arch. Surg.* **398**, 1–12 (2013).
104. T. Hattori, N. Arizono, Cell kinetics and secretion of mucus in the gastrointestinal mucosa, and their diurnal rhythm. *J. Clin. Gastroenterol.*, **10** (Suppl. 1), S1–S6 (1988).
105. J. F. Brooks II, C. L. Behrendt, K. A. Ruhn, S. Lee, P. Raj, J. S. Takahashi, L. V. Hooper, The microbiota coordinates diurnal rhythms in innate immunity with the circadian clock. *Cell* **184**, 4154–4167.e12 (2021).
106. W. Krugluger, A. Brandstaetter, E. Kállay, J. Schueller, E. Krexner, S. Kriwanek, E. Bonner, H. S. Cross, Regulation of genes of the circadian clock in human colon cancer: Reduced period-1 and dihydropyrimidine dehydrogenase transcription correlates in high-grade tumors. *Cancer Res.* **67**, 7917–7922 (2007).
107. G. Mazzoccoli, A. Panza, M. R. Valvano, O. Palumbo, M. Carella, V. Pazienza, G. Biscaglia, F. Tavano, P. Di Sebastiano, A. Andriulli, A. Piepoli, Clock gene expression levels and relationship with clinical and pathological features in colorectal cancer patients. *Chronobiol. Int.* **28**, 841–851 (2011).
108. G. Mazzoccoli, T. Colangelo, A. Panza, R. Rubino, A. De Cata, C. Tiberio, M. R. Valvano, V. Pazienza, G. Merla, B. Augello, D. Trombetta, C. T. Storlazzi, G. Macchia, A. Gentile, F. Tavano, M. Vinciguerra, G. Bisceglia, V. Rosato, V. Colantuoni, L. Sabatino, A. Piepoli, Deregulated expression of cryptochrome genes in human colorectal cancer. *Mol. Cancer* **15**, 6 (2016).
109. T. Oshima, S. Takenoshita, M. Akaike, C. Kunisaki, S. Fujii, A. Nozaki, K. Numata, M. Shiozawa, Y. Rino, K. Tanaka, M. Masuda, T. Imada, Expression of circadian genes correlates with liver metastasis and outcomes in colorectal cancer. *Oncol. Rep.* **25**, 1439–1446 (2011).
110. H. Zeng, D. L. Lazarova, M. Bordonaro, Mechanisms linking dietary fiber, gut microbiota and colon cancer prevention. *World J. Gastrointest. Oncol.* **6**, 41–51 (2014).
111. A. M. Caricilli, A. Castoldi, N. O. S. Câmara, Intestinal barrier: A gentlemen's agreement between microbiota and immunity. *World J. Gastrointest. Pathophysiol.* **5**, 18–32 (2014).
112. C. Chelakkot, J. Ghim, S. H. Ryu, Mechanisms regulating intestinal barrier integrity and its pathological implications. *Exp. Mol. Med.* **50**, 1–9 (2018).
113. L. Hu, G. Li, Y. Shu, X. Hou, L. Yang, Y. Jin, Circadian dysregulation induces alterations of visceral sensitivity and the gut microbiota in light/dark phase shift mice. *Front. Microbiol.* **13**, 935919 (2022).
114. K. Tanabe, E. Kitagawa, M. Wada, A. Haraguchi, K. Orihara, Y. Tahara, A. Nakao, S. Shibata, Antigen exposure in the late light period induces severe symptoms of food allergy in an OVA-allergic mouse model. *Sci. Rep.* **5**, 14424 (2015).
115. M. Yamato, T. Ito, H. Iwatani, M. Yamato, E. Imai, H. Rakugi, E-cadherin and claudin-4 expression has circadian rhythm in adult rat kidney. *J. Nephrol.* **23**, 102–110 (2010).
116. N. Hudson, L. Celkova, A. Hopkins, C. Greene, F. Storti, E. Ozaki, E. Fahey, S. Theodoropoulou, P. F. Kenna, M. M. Humphries, A. M. Curtis, E. Demmons, A. Browne, S. Liddie, M. S. Lawrence, C. Grimm, M. T. Cahill, P. Humphries, S. L. Doyle, M. Campbell, Dysregulated claudin-5 cycling in the inner retina causes retinal pigment epithelial cell atrophy. *JCI Insight* **4**, e130273 (2019).
117. E. M. M. Louer, D. Günzel, R. Rosenthal, C. Carmone, G. Yi, H. G. Stunnenberg, A. I. den Hollander, P. M. T. Deen, Differential day-night expression of tight junction components in murine retinal pigment epithelium. *Exp. Eye Res.* **193**, 107985 (2020).
118. R. B. van Breemen, Y. Li, Caco-2 cell permeability assays to measure drug absorption. *Expert Opin. Drug Metab. Toxicol.* **1**, 175–185 (2005).
119. J. L. Drewes, J. R. White, C. M. Dejea, P. Fathi, T. Iyadorai, J. Vadivelu, A. C. Roslani, E. C. Wick, E. F. Mongodin, M. F. Loke, K. Thulasi, H. M. Gan, K. L. Goh, H. Y. Chong, S. Kumar, J. W. Wanyiri, C. L. Sears, High-resolution bacterial 16S rRNA gene profile meta-analysis and biofilm status reveal common colorectal cancer consortia. *NPJ Biofilms Microbiomes* **3**, 34 (2017).
120. Y. Chen, Y. Chen, J. Zhang, P. Cao, W. Su, Y. Deng, N. Zhan, X. Fu, Y. Huang, W. Dong, *Fusobacterium nucleatum* promotes metastasis in colorectal cancer by activating autophagy signaling via the upregulation of CARD3 expression. *Theranostics* **10**, 323–339 (2020).

121. L. Flanagan, J. Schmid, M. Ebert, P. Soucek, T. Kunicka, V. Liska, J. Bruha, P. Neary, N. Dezeeuw, M. Tommasino, M. Jenab, J. H. M. Prehn, D. J. Hughes, *Fusobacterium nucleatum* associates with stages of colorectal neoplasia development, colorectal cancer and disease outcome. *Eur. J. Clin. Microbiol. Infect. Dis.* **33**, 1381–1390 (2014).
122. W. Chen, F. Liu, Z. Ling, X. Tong, C. Xiang, Human intestinal lumen and mucosa-associated microbiota in patients with colorectal cancer. *PLOS ONE* **7**, e39743 (2012).
123. Y.-N. Yu, T.-C. Yu, H.-J. Zhao, T.-T. Sun, H.-M. Chen, H.-Y. Chen, H.-F. An, Y.-R. Weng, J. Yu, M. Li, W.-X. Qin, X. Ma, N. Shen, J. Hong, J.-Y. Fang, Berberine may rescue *Fusobacterium nucleatum*-induced colorectal tumorigenesis by modulating the tumor microenvironment. *Oncotarget* **6**, 32013–32026 (2015).
124. V. Eklöf, A. Löfgren-Burström, C. Zingmark, S. Edin, P. Larsson, P. Karling, O. Alexeyev, J. Rutegård, M. L. Wikberg, R. Palmqvist, Cancer-associated fecal microbial markers in colorectal cancer detection. *Int. J. Cancer* **141**, 2528–2536 (2017).
125. Y. Suehiro, K. Sakai, M. Nishioka, S. Hashimoto, T. Takami, S. Higaki, Y. Shindo, S. Hazama, M. Oka, H. Nagano, I. Sakaida, T. Yamasaki, Highly sensitive stool DNA testing of *Fusobacterium nucleatum* as a marker for detection of colorectal tumours in a Japanese population. *Ann. Clin. Biochem.* **54**, 86–91 (2017).
126. S. H. Wong, T. N. Y. Kwong, T.-C. Chow, A. K. C. Luk, R. Z. W. Dai, G. Nakatsu, T. Y. T. Lam, L. Zhang, J. C. Y. Wu, F. K. L. Chan, S. S. M. Ng, M. C. S. Wong, S. C. Ng, W. K. K. Wu, J. Yu, J. J. Y. Sung, Quantitation of faecal *Fusobacterium* improves faecal immunochemical test in detecting advanced colorectal neoplasia. *Gut* **66**, 1441–1448 (2017).
127. S. Guo, L. Li, B. Xu, M. Li, Q. Zeng, H. Xiao, Y. Xue, Y. Wu, Y. Wang, W. Liu, G. Zhang, A simple and novel fecal biomarker for colorectal cancer: Ratio of *Fusobacterium Nucleatum* to probiotics populations, based on their antagonistic effect. *Clin. Chem.* **64**, 1327–1337 (2018).
128. S. Wang, Y. Liu, J. Li, L. Zhao, W. Yan, B. Lin, X. Guo, Y. Wei, *Fusobacterium nucleatum* acts as a pro-carcinogenic bacterium in colorectal cancer: From association to causality. *Front. Cell Dev. Biol.* **9**, 710165 (2021).
129. Y. Zhang, J. Shen, X. Shi, Y. Du, Y. Niu, G. Jin, Z. Wang, J. Lyu, Gut microbiome analysis as a predictive marker for the gastric cancer patients. *Appl. Microbiol. Biotechnol.* **105**, 803–814 (2021).
130. N. Li, C. Bai, L. Zhao, Z. Sun, Y. Ge, X. Li, The relationship between gut microbiome features and chemotherapy response in gastrointestinal cancer. *Front. Oncol.* **11**, 781697 (2021).
131. M. S. Rye, K. L. Garrett, R. A. Holt, C. F. Platell, M. J. McCoy, *Fusobacterium nucleatum* and *Bacteroides fragilis* detection in colorectal tumours: Optimal target site and correlation with total bacterial load. *PLOS ONE* **17**, e0262416 (2022).
132. R. J. Knippel, J. L. Drewes, C. L. Sears, The cancer microbiome: Recent highlights and knowledge gaps. *Cancer Discov.* **11**, 2378–2395 (2021).
133. J. Puschhof, E. Elinav, Human microbiome research: Growing pains and future promises. *PLoS Biol.* **21**, e3002053 (2023).
134. H. M. Wexler, *Bacteroides*: The good, the bad, and the nitty-gritty. *Clin. Microbiol. Rev.* **20**, 593–621 (2007).
135. S. M. Bloom, V. N. Bijanki, G. M. Nava, L. Sun, N. P. Malvin, D. L. Donermeyer, W. M. Dunne, P. M. Allen, T. S. Stappenbeck, Commensal *Bacteroides* species induce colitis in host-genotype-specific fashion in a mouse model of inflammatory bowel disease. *Cell Host Microbe* **9**, 390–403 (2011).
136. J. L. Sonnenburg, J. Xu, D. D. Leip, C.-H. Chen, B. P. Westover, J. Weatherford, J. D. Buhler, J. I. Gordon, Glycan foraging in vivo by an intestine-adapted bacterial symbiont. *Science* **307**, 1955–1959 (2005).
137. M. S. Desai, A. M. Seekatz, N. M. Koropatkin, N. Kamada, C. A. Hickey, M. Wolter, N. A. Pudlo, S. Kitamoto, N. Terrapon, A. Muller, V. B. Young, B. Henrissat, P. Wilmes, T. S. Stappenbeck, G. Núñez, E. C. Martens, A dietary fiber-deprived gut microbiota degrades the colonic mucus barrier and enhances pathogen susceptibility. *Cell* **167**, 1339–1353.e21 (2016).
138. S. Qu, Y. Zheng, Y. Huang, Y. Feng, K. Xu, W. Zhang, Y. Wang, K. Nie, M. Qin, Excessive consumption of mucin by over-colonized *Akkermansia muciniphila* promotes intestinal barrier damage during malignant intestinal environment. *Front. Microbiol.* **14**, 1111911 (2023).
139. Y. Zhang, J. Zhang, Y. Xia, J. Sun, Bacterial translocation and barrier dysfunction enhance colonic tumorigenesis. *Neoplasia* **35**, 100847 (2023).
140. C. E. Bailey, C.-Y. Hu, Y. N. You, B. K. Bednarski, M. A. Rodriguez-Bigas, J. M. Skibber, S. B. Cantor, G. J. Chang, Increasing disparities in the age-related incidences of colon and rectal cancers in the United States, 1975-2010. *JAMA Surg.* **150**, 17–22 (2015).
141. I. Ben-Aharon, H. W. M. van Laarhoven, E. Fontana, R. Obermannova, M. Nilsson, F. Lordick, Early-onset cancer in the gastrointestinal tract is on the rise-evidence and implications. *Cancer Discov.* **13**, 538–551 (2023).
142. F. A. Sinicrope, Increasing incidence of early-onset colorectal cancer. *N. Engl. J. Med.* **386**, 1547–1558 (2022).
143. A. F. Cheung, A. M. Carter, K. K. Kostova, J. F. Woodruff, D. Crowley, R. T. Bronson, K. M. Haigis, T. Jacks, Complete deletion of Apc results in severe polyposis in mice. *Oncogene* **29**, 1857–1864 (2010).
144. K.-F. Storch, C. Paz, J. Signorovitch, E. Raviola, B. Pawlyk, T. Li, C. J. Weitz, Intrinsic circadian clock of the mammalian retina: Importance for retinal processing of visual information. *Cell* **130**, 730–741 (2007).
145. B. B. Madison, L. Dunbar, X. T. Qiao, K. Braunstein, E. Braunstein, D. L. Gumucio, Cis elements of the villin gene control expression in restricted domains of the vertical (crypt) and horizontal (duodenum, cecum) axes of the intestine. *J. Biol. Chem.* **277**, 33275–33283 (2002).
146. A. M. Bolger, M. Lohse, B. Usadel, Trimmomatic: A flexible trimmer for Illumina sequence data. *Bioinformatics* **30**, 2114–2120 (2014).
147. D. Kim, L. Song, F. P. Breitwieser, S. L. Salzberg, Centrifuge: Rapid and sensitive classification of metagenomic sequences. *Genome Res.* **26**, 1721–1729 (2016).
148. T. Sato, R. G. Vries, H. J. Snippert, M. van de Wetering, N. Barker, D. E. Stange, J. H. van Es, A. Abo, P. Kujala, P. J. Peters, H. Clevers, Single Lgr5 stem cells build crypt-villus structures in vitro without a mesenchymal niche. *Nature* **459**, 262–265 (2009).
149. T. Zieliński, J. Hay, A. J. Millar, "Period estimation and rhythm detection in timeseries data using biodare2, the free, online, community resource" in *Plant Circadian Networks: Methods and Protocols*, D. Staiger, S. Davis, A. M. Davis, Eds. (Springer, 2022), pp. 15–32.
150. M. I. Love, W. Huber, S. Anders, Moderated estimation of fold change and dispersion for RNA-seq data with DESeq2. *Genome Biol.* **15**, 550 (2014).
151. N. G. Lamson, R. L. Ball, K. C. Fein, K. A. Whitehead, Thrifty, rapid intestinal monolayers (TRIM) using caco-2 epithelial cells for oral drug delivery experiments. *Pharm. Res.* **36**, 172 (2019).

Acknowledgments: We wish to thank all members of the Masri lab for discussion and feedback on the project. We acknowledge the support of the Chao Family Comprehensive Cancer Center (CFCCC) at the University of California, Irvine, which is supported by the National Institutes of Health (NIH)/National Cancer Institute (NCI) (grant no. P30 CA062203). Shared resources utilized through the CFCCC include the Experimental Tissue Resource (ETR). **Funding:** The Pannunzio lab is supported by NIH grants R37 CA266042 and R01 CA276470. The Seldin lab is supported by NIH grant DP1 DK130640. Financial support for the Masri laboratory is provided through the NIH (grants R01 CA244519 and R01 CA259370), the Concern Foundation, Johnson and Johnson, and support from the Anti-Cancer Challenge through the CFCCC. B.M.F. is supported by funds through NIH/NCI (grant no. T32CA009054 and F31CA287992) and support through Estée Lauder. A.L.M. is supported by the National Science Foundation Graduate Research Fellowship Program (grant DGE-1839285). **Author contributions:** Conceptualization: S.M., R.C.F., and A.L.M. Methodology: S.M., R.C.F., S.K.C., N.L., B.M.F., M.M.S., and N.R.P. Resources: A.L.M., W.A.S., N.R.P., and S.M. Funding acquisition: S.M. Data Curation: N.L. and S.M. Validation: S.K.C., N.L., B.M.F., and S.M. Supervision: S.M. Project administration: S.M. Visualization: R.C.F., N.L., W.A.S., and S.M. Investigation: R.C.F., S.K.C., N.L., B.M.F., A.L.M., and W.A.S. Formal analysis: S.K.C., N.L., and N.R.P. Software: N.L. Writing—original draft: R.C.F., A.L.M., and S.M. Writing—review and editing: R.C.F., S.K.C., N.L., B.M.F., A.L.M., W.A.S., and S.M. **Competing interests:** The authors declare that they have no competing interests. **Data and materials availability:** All data needed to evaluate the conclusions in the paper are present in the paper and/or the Supplementary Materials. Microbiome sequencing data are available in the Sequence Read Archive (SRA) under the BioProject accession number PRJNA1025260. Previously published RNA-seq data are available in the SRA under the BioProject accession number PRJNA767410.

Submitted 19 January 2024
Accepted 22 August 2024
Published 27 September 2024
10.1126/sciadv.ado1458